ARTICLE

doi:10.1038/nature22341

Exosomes facilitate therapeutic targeting of oncogenic KRAS in pancreatic cancer

Sushrut Kamerkar[1], Valerie S. LeBleu[1], Hikaru Sugimoto[1], Sujuan Yang[1], Carolina F. Ruivo[2], Sonia A. Melo[1,2], J. Jack Lee[3] & Raghu Kalluri[1]

The mutant form of the GTPase KRAS is a key driver of pancreatic cancer but remains a challenging therapeutic target. Exosomes are extracellular vesicles generated by all cells, and are naturally present in the blood. Here we show that enhanced retention of exosomes, compared to liposomes, in the circulation of mice is likely due to CD47–mediated protection of exosomes from phagocytosis by monocytes and macrophages. Exosomes derived from normal fibroblast–like mesenchymal cells were engineered to carry short interfering RNA or short hairpin RNA specific to oncogenic *Kras*^{G12D}, a common mutation in pancreatic cancer. Compared to liposomes, the engineered exosomes (known as iExosomes) target oncogenic KRAS with an enhanced efficacy that is dependent on CD47, and is facilitated by macropinocytosis. Treatment with iExosomes suppressed cancer in multiple mouse models of pancreatic cancer and significantly increased overall survival. Our results demonstrate an approach for direct and specific targeting of oncogenic KRAS in tumours using iExosomes.

Pancreatic ductal adenocarcinoma (PDAC) is in urgent need of effective new therapies[1]. Mutations in the GTPase KRAS are commonly encountered in PDAC[2] and these drive initiation, progression and metastasis[3,4]. Dampening oncogenic Kras using genetic manipulation in mice inhibits tumour progression despite the presence of other genetic defects[5]. A direct and specific targeting of RAS family proteins has however been elusive[6].

RNA interference (RNAi)-based approaches to target wild-type Kras or downstream effectors using nanoparticles showed an effect on tumour burden in lung and colorectal cancer models[7–9]. Targeting oncogenic KRAS has been limited to delivery via direct electroporation[10] or biopolymeric implants[11] in xenograft models of pancreatic cancer, and effective delivery of RNAi to non-liver parenchymal organs, especially the pancreas, remains a challenge. Although liposomes and nanoparticles may offer advantages for RNAi delivery over viral-based delivery systems, they exhibit low efficiency and rapid clearance from the circulation[12]. Here we investigated whether exosomes can function as efficient carriers of RNAi. Exosomes are nano-sized extracellular vesicles (40–150 nm) with a membrane lipid bilayer that are released by all cells and efficiently enter other cells[13].

Unlike liposomes and other synthetic drug nanoparticle carriers, exosomes contain transmembrane and membrane-anchored proteins that may enhance endocytosis, thus promoting the delivery of their internal content[14,15]. Exosomal proteins include CD47 (refs 16, 17), a widely expressed integrin-associated transmembrane protein that functions in part to protect cells from phagocytosis[18,19]. CD47 is the ligand for signal regulatory protein alpha (SIRPα, also known as CD172a), and CD47–SIRPα binding initiates the 'don't eat me' signal that inhibits phagocytosis[20]. Oncogenic RAS was shown to endow pancreatic cancer cells with enhanced macropinocytosis that may facilitate the cellular uptake of exosomes[21]. The use of exosomes might also minimize the cytotoxic effects that were observed when synthetic nanoparticles were used *in vivo*[22]. We identified the functional contribution of CD47 and oncogenic KRAS-stimulated macropinocytosis in suppressing exosomes clearance from the circulation and enhancing specificity to pancreatic cancer cells, respectively. Such properties of exosomes enhanced their ability to deliver RNAi to specifically target oncogenic KRAS in pancreatic tumours, and the use of exosomes as single targeted agents significantly improved the overall survival of all mouse models of PDAC tested.

CD47 suppresses exosome clearance by monocytes

Exosomes were purified from the supernatant of normal human foreskin fibroblast (BJ) cultures (Extended Data Fig. 1a, b). CD47 detection on exosomes is noted in mass spectrometry analysis of exosomes (Supplementary Table 1, ExoCarta database, http://exocarta.org). In contrast with liposomes, BJ fibroblasts exosomes were positive for CD63 and CD47, and exosomes derived from CD47-knockout mouse ear fibroblasts lacked CD47 (Extended Fig. 1c, d). We optimized the electroporation of Alexa Fluor 647 (AF647)-tagged short interfering RNA (siRNA) into exosomes (iExosomes) and liposomes (iLiposomes) without compromising their structural integrity (Extended Fig. 1a, e). Fractionation using a sucrose gradient revealed detection of AF647, indicative of siRNA, in fractions characteristic of exosomes and liposomes, whereas electroporated siRNA alone (siRNA was mixed with electroporation buffer and subjected to electroporation without exosomes or liposomes) did not accumulate in these fractions (Fig. 1a, Extended Data Fig. 1f, g). After intraperitoneal injection (24 h), iExosomes but not iLiposomes were detected in the circulation of either C57BL/6 or nude mice (Extended Fig. 2a, b). Three hours after intraperiteoneal injection, exosomes were also readily detected in the circulation, and although CD47-knockout exosomes showed diminished retention, exosomes with high levels of CD47 expression (CD47^{high} exosomes; see Methods) showed higher retention in the circulation (Fig. 1b, Extended Data Fig. 2c). Exosomes accumulated in the liver, lung and pancreas (Fig. 1c, Extended Data Fig. 2d), and a greater number of pancreatic cells showed an AF647-siRNA signal from iExosomes compared to iLiposomes (Fig. 1d, Extended Fig. 2e, f).

Generally, efficient phagocytosis by circulating monocytes and other cells removes dying and dead cells, cell debris and foreign particles.

[1]Department of Cancer Biology, Metastasis Research Center, University of Texas MD Anderson Cancer Center, Houston, Texas 77005, USA. [2]Instituto de Investigação e Inovação em Saúde, Universidade do Porto, Portugal (I3S), 4200 Porto, Portugal; Institute of Pathology and Molecular Immunology of the University of Porto (IPATIMUP), 4200 Porto, Portugal. [3]Department of Biostatistics, University of Texas MD Anderson Cancer Center, Houston, Texas 77005, USA.

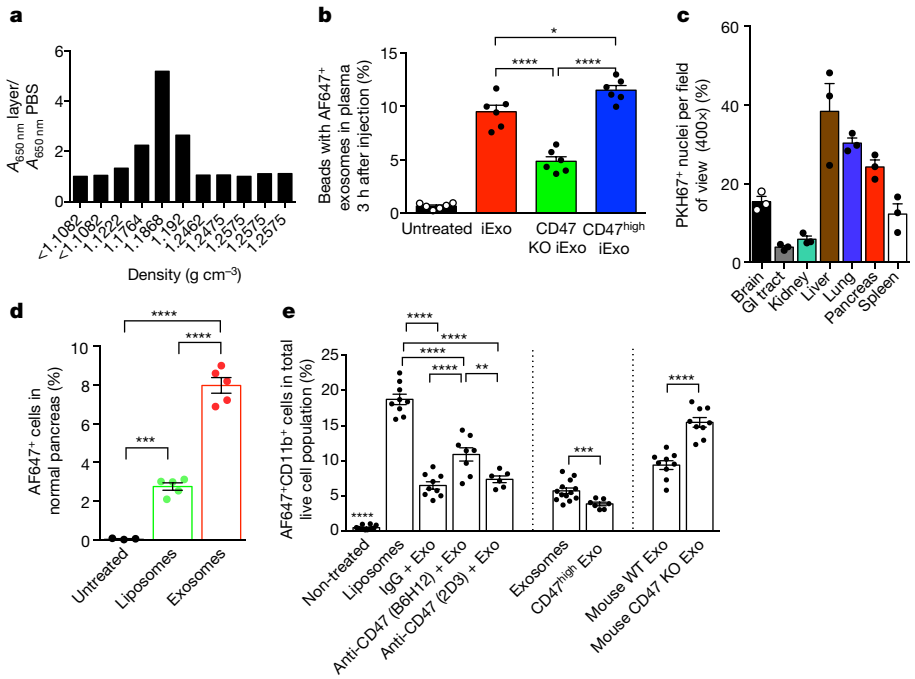

Figure 1 | CD47 on exosomes limits their clearance by circulating monocytes. a, Fluorescence intensity in sucrose gradient layers from 'bottom-up' method (see Supplementary Fig. 1e, f). **b**, Flow cytometry analysis of exosomes with AF647-tagged siRNA (iExo) in the circulation. KO, knockout. $n = 6$ mice per group. **c**, Quantification of PKH67-labelled exosomes in the indicated organs. GI, gastrointestinal. $n = 3$ mice per group. **d**, Flow cytometry analyses of pancreas cells 6 h after injection of siKras^{G12D} exosomes or liposomes (both $n = 5$ mice), or PBS (untreated, $n = 3$ mice), measured by AF647-positivity. **e**, Quantification of AF647^{+}CD11b^{+} monocytes in the blood 3 h after intraperitoneal injection. $n = 12$ mice (non-treated); $n = 9$ mice (liposomes, IgG + siKras^{G12D} exosomes, mouse wild-type (WT) exosomes, mouse CD47-knockout exosomes); $n = 8$ mice (anti-CD47 (B6H12) + siKras^{G12D} exosomes); $n = 6$ mice (anti-CD47 (2D3) + siKras^{G12D} exosomes); $n = 13$ mice (exosomes: siKras^{G12D} exosomes); $n = 7$ mice (CD47^{high} Exo: CD47^{high} siKras^{G12D} exosomes). Data are mean ± s.e.m. $*P < 0.05$, $**P < 0.01$, $***P < 0.001$, $****P < 0.0001$, one-way ANOVA (**b**, **d**, **e**) and unpaired two-tailed t-test (in **e**, exosomes versus CD47^{high} exo; mouse wild-type versus CD47-knockout exosomes). See accompanying Source Data.

iLiposomes, compared to iExosomes, enhanced the mobilization of CD11b^{+} monocytes in the circulation (Extended Data Fig. 3a, b). While control mouse blood (untreated) showed background levels of AF647 positivity in CD11b^{+} monocytes, an increase in the number of circulating AF647^{+} monocytes (indicative of phagocytosis) was noted when mice were treated with liposomes rather than exosomes (Fig. 1e, Extended Data Fig. 3c). Furthermore, the levels of CD47 on exosomes inversely correlated with circulating AF647^{+} monocytes in the blood (Fig. 1e, Extended Data Fig. 3c), supporting the idea that the presence of CD47 on exosomes limits their clearance. Furthermore, after the injection of iExosomes, the AF647^{+} monocytes in the circulation were positive for SIRPα (Extended Data Fig. 3d). Using an anti-CD47 (clone B6H12) blocking antibody, which prevents CD47/SIRPα inhibition of phagocytosis in contrast with non-blocking anti-CD47 (clone 2D3) antibody[23], resulted in a specific and significant increase in AF647^{+}CD11b^{+} circulating monocytes (Fig. 1e, Extended Data Fig. 3c). Notably, the binding of anti-CD47 (2D3) and anti-CD47 (B6H12) antibodies to exosomes was similar (Extended Data Fig. 3e). By contrast, decreased AF647^{+}CD11b^{+} circulating monocytes were noted when using CD47^{high} iExosomes (Fig. 1e, Extended Data Fig. 3c). Interestingly, CD47-knockout mice showed lower levels of circulating exosomes compared to age-matched controls (Extended Data Fig. 3f). Our results indicated a superior escape from phagocytic clearance of exosomes compared to liposomes, in part mediated by the exosomal CD47–SIRPα 'don't eat me' signal.

Specific targeting of *KRAS*^{G12D} using iExosomes

iExosomes (with siRNA or shRNA targeting *KRAS*^{G12D}) significantly reduced *KRAS*^{G12D} mRNA levels and phosphorylated-ERK protein levels in human PANC-1 cells, with superior efficacy compared to iLiposomes, despite a similar siRNA loading efficiency in both nanoparticles (Extended Data Fig. 4a–h, Supplementary Information, Supplementary Fig. 1). iExosomes also suppressed RAS activity specifically in PANC-1 cells compared to human BxPC-3 cells (*KRAS* wild-type) (Extended Data Fig. 4i, Supplementary Fig. 2), and impaired proliferation (Extended Data Fig. 4j, k) and enhanced apoptosis (Extended Data Fig. 4l–n) in PANC-1 cells, while leaving BxPC-3 (*KRAS* wild type), Capan-1 (*KRAS*^{G12V}) and MIA PaCa-2 (*KRAS*^{G12C}) cancer cells unaffected (Extended Data Fig. 4o–u).

iExosomes suppress Kras^{G12D} orthotopic tumours

Mice with luciferase-expressing orthotopic PANC-1 tumours were treated with repeated intraperitoneal injections of approximately 10^8 iExosomes (0.15–0.20 μg of exosomal protein per injection) or iLiposomes every other day (Extended Data Fig. 5a). Accumulation of iExosome payloads (AF647-siRNA) was readily detected in the pancreas (Extended Data Fig. 5b). Although the tumours of control mice (PBS vehicle, non-electroporated exosomes, or exosomes and liposomes with scrambled RNAi) grew at an exponential rate, the tumours treated with iExosomes were significantly reduced after 30 days of treatment (Extended Data Fig. 5c). Tumour growth was blunted with iLiposomes, however, to a much lesser extent than with iExosomes (Extended Data Fig. 5c).

When control mice revealed extensive tumour burden, tumours in iExosome-treated mice were in contrast reduced to nearly undetectable levels (Fig. 2a, b, Extended Data Fig. 5d, e), and this persisted after 200 days of treatment (Fig. 2c, Extended Data Fig. 5f). Histopathological end-point analyses, relative pancreas mass, and overall survival indicated robust improvement in iExosome-treated mice (Fig. 2c–e, Extended Data Fig. 5g). iExosomes suppressed downstream KRAS signalling and *KRAS*^{G12D} expression in tumours and the pancreas

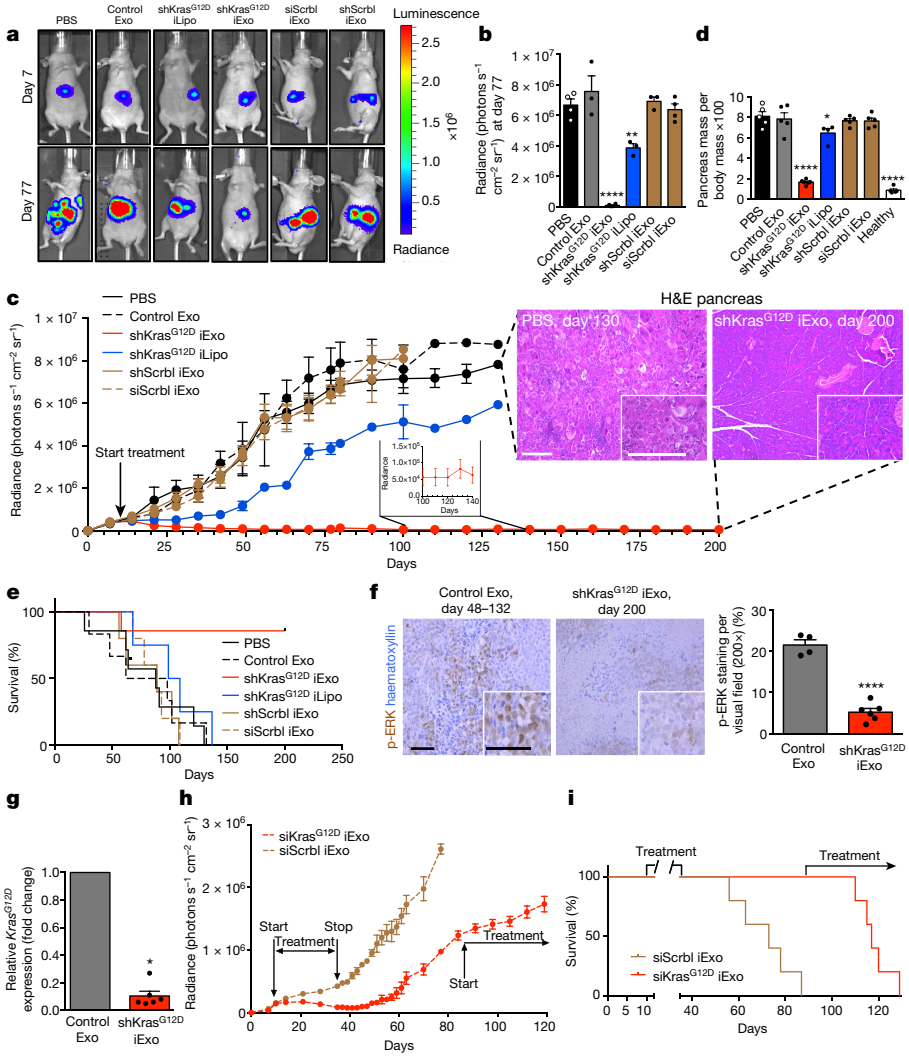

Figure 2 | iExosomes restrains PANC-1 tumour growth. a, Luciferase activity at days 7 and 77 after cancer cell injection. shScrbl and siScrbl denote scrambled shRNA and siRNA controls, respectively. **b**, Tumour bioluminescence at day 77. $n = 4$ mice (PBS, shKras^{G12D} iLipo); $n = 3$ mice (control Exo); $n = 6$ mice (shKras^{G12D} iExo); $n = 5$ mice (shScrbl iExo, siScrbl iExo). **c**, Left, PANC-1 orthotopic tumour growth (bioluminescence). $n = 7$ mice (PBS, shKras^{G12D} iExo); $n = 6$ mice (control Exo); $n = 4$ mice (shKras^{G12D} iLipo); $n = 5$ mice (shScrbl iExo, siScrbl iExo). Right, representative haematoxylin and eosin (H&E) staining of the pancreas. Scale bars, 100 μm. **d**, Relative pancreas mass. $n = 5$ mice (PBS, shScrbl iExo, siScrbl iExo, control Exo); $n = 6$ mice (shKras^{G12D} iExo); $n = 4$ mice (shKras^{G12D} iLipo). **e**, Kaplan–Meier survival curve of PANC-1 tumour-bearing mice. $n = 7$ mice (PBS, shKras^{G12D} iExo); $n = 6$ mice (control Exo); $n = 4$ mice (shKras^{G12D} iLipo); $n = 5$ mice (shScrbl iExo, siScrbl iExo). shKras^{G12D} iExo-treated mice showed a significant increase in survival when compared to every other treatment group ($P < 0.05$, log-rank Mantel–Cox test). **f**, Phosphorylated-ERK (p-ERK) immunolabelling. Scale bars, 100 μm. $n = 4$ mice (control Exo); $n = 6$ mice (shKras^{G12D} iExo). **g**, *Kras^{G12D}* transcript levels in tumours. $n = 5$ mice (control Exo); $n = 6$ mice (shKras^{G12D} iExo). **h**, PANC-1 orthotopic tumour growth (bioluminescence). $n = 5$ mice per group. **i**, Kaplan–Meier survival curve of PANC-1 tumour-bearing mice. $P < 0.01$, log-rank Mantel–Cox test. $n = 5$ mice per group. Data are mean ± s.e.m. $^{*}P < 0.05$, $^{**}P < 0.01$, $^{***}P < 0.001$, $^{****}P < 0.0001$, ANOVA compared to control (PBS) (**b**, **d**,) and unpaired two-tailed *t*-test (**f**, **g**). See accompanying Source Data.

(Fig. 2f, g, Extended Fig. 5h). Suspending iExosome treatment after initial tumour reduction showed sustained tumour suppression effects that lasted more than 10 days after the last treatment with iExosomes (Fig. 2h). Control mice succumbed to pancreatic cancer, whereas the mice treated with siKras^{G12D} iExosomes were all alive (day 87). Resuming iExosome treatment at this point controlled the growth of these advanced tumours (Fig. 2h, i). Despite continuous treatment at an advanced disease state, the mice responded with partial tumour growth control but ultimately succumbed (Fig. 2h, i). iExosomes did not, however, affect orthotopic BxPC-3 (*KRAS* wild type) tumour growth or survival (Extended Data Fig. 5i–m). Loss of surface proteins on exosomes with proteinase K treatment, validated by flow cytometry (Extended Data Fig. 6a), significantly suppressed the anti-tumour efficacy of iExosomes, whereas RNase A treatment alone did not have any effect (Extended Data Fig. 6b–j, Supplementary Information).

CD47 and macropinocytosis facilitate iExosome efficacy

In mice with orthotopic PANC-1 tumours, iExosomes and iLiposomes were administered with or without incubation with anti-CD47 neutralizing antibodies. Unlike with iLiposomes or anti-CD47 antibodies alone, the efficacy of iExosomes was significantly inhibited by neutralization of the CD47–SIRPα 'don't eat me' signal (Fig. 3a, Extended Fig. 6k–m, Supplementary Fig. 4c). In immunocompetent mice with orthotopic tumours from the KPC689 cancer cell line (see Methods), CD47-knockout iExosomes failed to suppress tumour growth robustly and improve survival compared to iExosomes (Fig. 3b, c, Extended Fig. 6n, o). In this model (treatment start 16 days after cancer cell injection), iLiposomes and control treatment were ineffective (Fig. 3b, c, Extended Data Fig. 6n, o). Similar results were obtained when performing the experiments in nude mice, despite a more aggressive cancer progression in the immunocompromised background (Extended Fig. 6p–r).

Accumulation of PKH67-labelled exosome signal (fluorescent lipophilic dye) was predominantly detected in established PANC-1 tumours 3 h after the injection, with less efficient accumulation noted in adjacent normal pancreas (Fig. 3d). Accumulation of AF647^{+} foci (iExosomes) was observed in *Ptf1a$^{cre/+}$;LSL-Kras$^{G12D/+}$;Tgfbr2$^{lox/lox}$* (KTC) mice, predominantly in tumours cells, as well as in normal acini, ducts, endocrine islet and α-smooth muscle actin (α-SMA)$^{+}$ cancer-associated fibroblasts (Extended Data Fig. 7a). Notably, decreased AF647^{+} foci in pancreas tumours was noted when using CD47-knockout iExosomes compared to wild-type iExosomes (Extended Data Fig. 7b). Collectively, these data suggested that along with enhanced retention of iExosomes in the systemic circulation, increased accumulation of iExosomes in tumours could reflect enhanced uptake of iExosomes in cancer cells when compared to normal pancreatic cells. This observation further complements the *in vitro* studies that demonstrate that exosomes deliver RNAi molecules to the pancreatic cancer cells more efficiently than liposomes (Extended Data Fig. 4a–h). In this regard, oncogenic RAS has been implicated in intensifying macropinocytosis[21,24]. Our results confirmed increased macropinocytosis in PANC-1 cells compared to BxPC-3 cells (Fig. 3e, Extended Fig. 7c, d). Exosome uptake mirrored the macropinocytosis frequency,

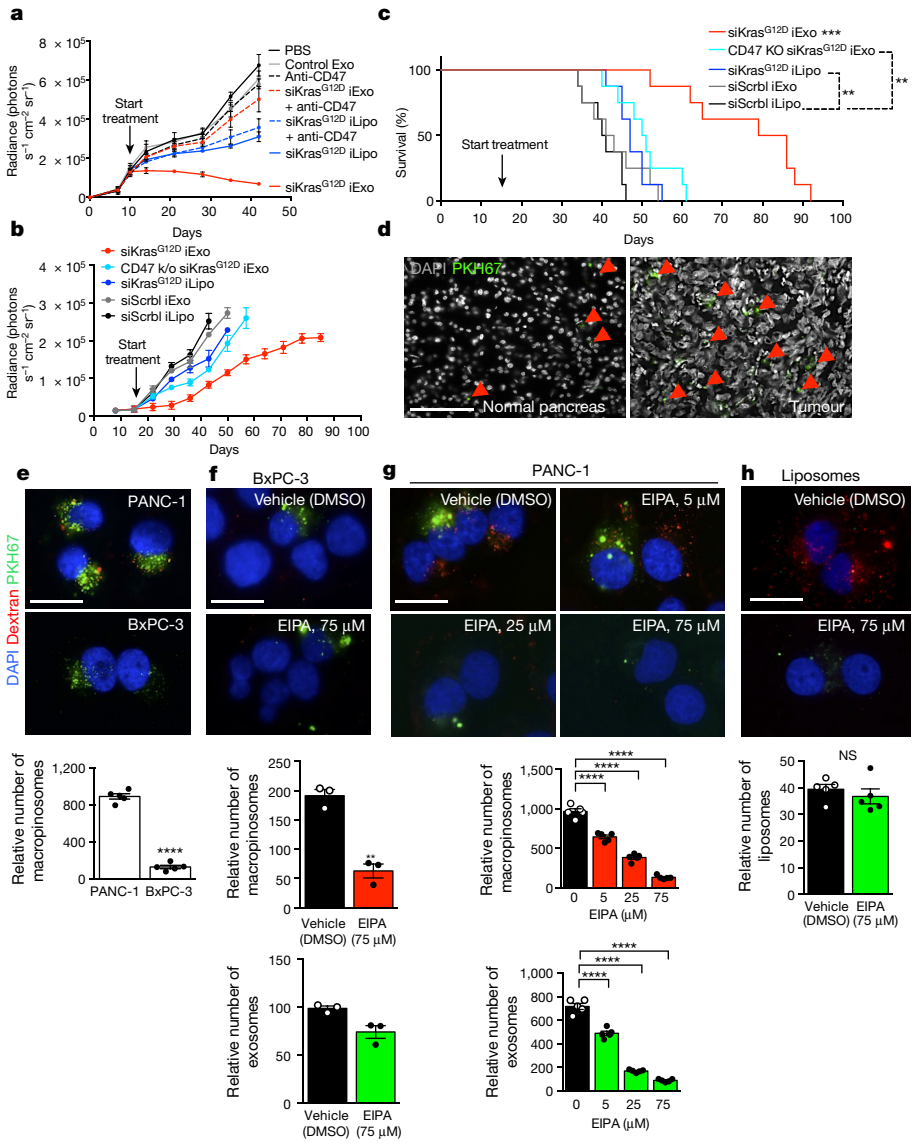

Figure 3 | CD47 and macropinocytosis enhance iExosomes uptake and therapeutic efficacy. a, PANC-1 orthotopic tumour growth (bioluminescence). $n = 3$ mice per group. **b**, KPC689 orthotopic tumour growth (bioluminescence). $n = 8$ mice per group. **c**, Kaplan–Meier survival curve, KPC689 orthotopic tumour-bearing mice. $n = 8$ mice per group. **d**, Confocal micrographs of increased (preferential) entry of labelled exosomes into tumour tissue. **e**, Macropinocytic uptake in PANC-1 or BxPC-3 cells. **f**, **g**, Macropinocytic and exosomes uptake in BxPC-3 (**f**) or PANC-1 (**g**) cells treated with vehicle (dimethylsulfoxide, DMSO) or EIPA at the indicated concentrations. **h**, Macropinosome and liposome uptake. Data are from 5 (**e**, **g**, **h**) or 3 (**f**) distinct wells. Scale bars, 100 μm (**d**) and 50 μm (**e**–**h**). Data are mean ± s.e.m. NS, not significant; $*P < 0.05$, $**P < 0.01$, $***P < 0.001$, $****P < 0.0001$, log-rank Mantel–Cox test (**c**), unpaired two-tailed *t*-test (**e**, **f**, **h**), one-way ANOVA (**g**). See accompanying Source Data.

and inhibition of macropinocytosis with 5-(*N*-ethyl-*N*-isopropyl) amiloride (EIPA) reduced exosome but not liposome uptake (Fig. 3f–h, Extended Fig. 7c, d). Treatment of exosomes with proteinase K or trypsin significantly reduced their entry into PANC-1 cells, yet this was independent of CD47 (Extended Data Fig. 7e–g). Three distinct mechanisms thus probably contribute to the enhanced anti-tumour response to iExosomes: CD47 presence on exosomes contributes to evasion from the host immune clearance in the circulation, RAS-mediated enhanced macropinocytosis, and the presence of proteins on the surface of exosomes that may increase pancreatic cancer cells uptake of iExosomes.

iExosomes inhibit metastasis and increase survival

We treated KTC mice[25,26] with iExosomes on day 18 (early treatment start) or day 33 (late treatment start) when mice present with PDAC (Extended Data Fig. 8a). Notably, accumulation of the AF647-siRNA signal was detected in KTC tumours (Extended Data Fig. 8b). In both experiments, iExosomes had an increased lifespan compared to control exosomes (Fig. 4a, b), in contrast with a lack of response observed when mice were treated with gemcitabine (Extended Fig. 8c and shown by others[25,27–29]). iExosomes reduced the tumour burden (Fig. 4c, d, Extended Data Fig. 8d) and improved histopathology (Fig. 4e, Extended Data Fig. 8e). iExosomes from human or mouse sources showed similar response (Extended Data Fig. 8f, g). Diminished pancreas desmoplasia, enhanced cancer cell apoptosis, suppressed cancer cell proliferation, reduced phosphorylated-ERK, phosphorylated-AKT and Kras levels are noted in KTC tumours, as well as diminished oncogenic *Kras*^{G12D} expression with iExosomes treatment (Fig. 4f, g, Extended Data Fig. 8h). Before the start of treatment, *Pdx1*$^{cre/+}$;*LSL-Kras*$^{G12D/+}$;*LSL-Trp53*$^{R172H/+}$ (KPC) mice showed comparable tumour burden (Fig. 4h), and iExosomes in this model also showed anti-tumour efficacy with increased survival (Fig. 4i). Furthermore, no obvert cytotoxicity was observed with iExosomes therapy (Extended Fig. 9a–c). iExosomes also suppressed PDAC progression in the advanced,

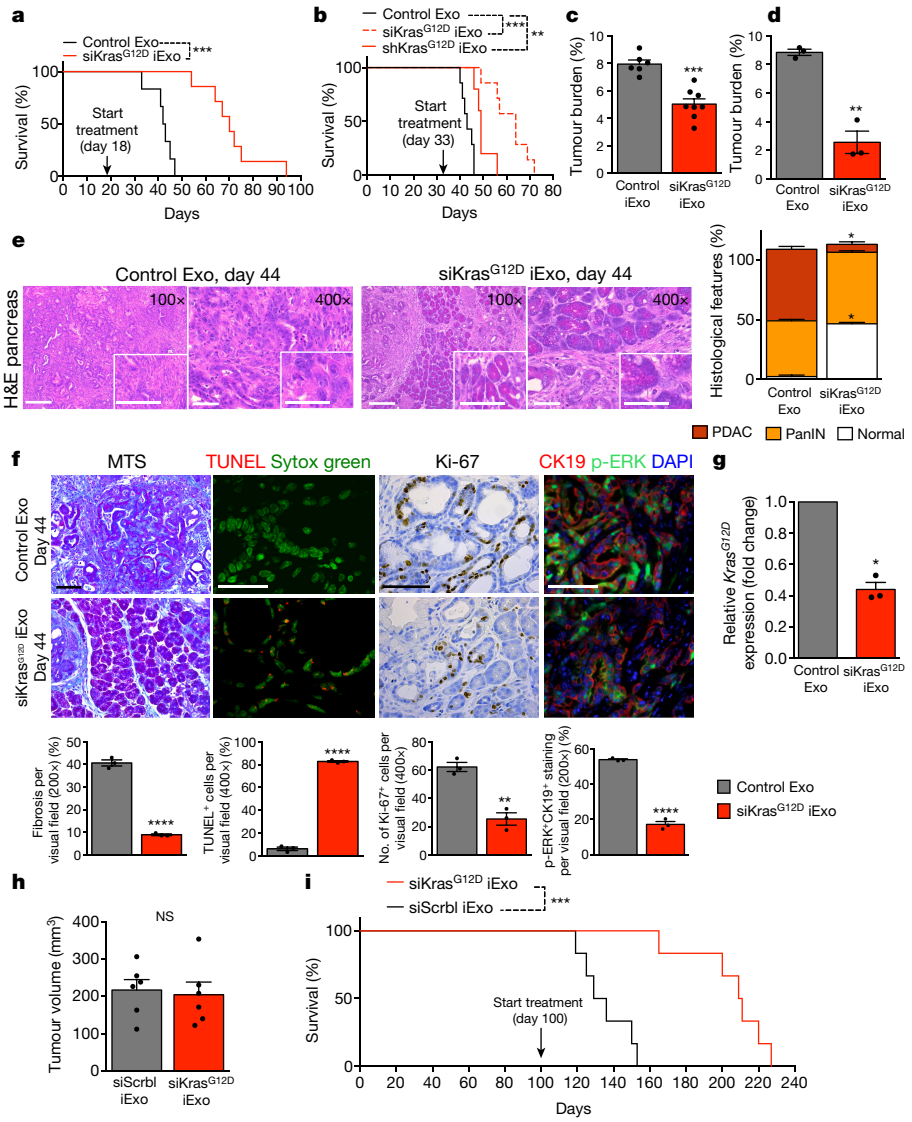

Figure 4 | iExosomes suppress pancreatic cancer progression in KTC and KPC genetically engineered mouse models. a, Kaplan–Meier survival curve of KTC (early treatment) mice. $n = 8$ mice (siKras^{G12D} iExo); $n = 6$ mice (control Exo). **b**, Kaplan–Meier survival curve of KTC mice. $n = 7$ mice (siKras^{G12D} iExo, control Exo); $n = 5$ mice (shKras^{G12D} iExo). **c**, Tumour burden (early treatment) at the experimental end point. $n = 8$ mice (siKras^{G12D} iExo); $n = 6$ mice (control Exo). **d**, Tumour burden at 44 days of age. $n = 3$ mice per group. **e**, H&E-stained tumours from 44-day-old KTC mice and relative percentages in histological phenotypes. PanIN, pancreatic intraepithelial neoplasia. $n = 3$ mice per group. **f**, Masson's trichrome staining (MTS), TUNEL, Ki-67, and p-ERK and CK19 immunolabelling of 44-day-old KTC mice. $n = 3$ mice per group. **g**, *Kras^{G12D}* transcript levels in tumours of age-matched (44-day-old) KTC mice. $n = 3$ mice per group. **h**, Tumour volume at baseline (determined by magnetic resonance imaging; MRI). $n = 6$ mice per group. **i**, Kaplan–Meier curve of KPC mice. $n = 6$ mice per group. Scale bars, 100 μm and 50 μm (**e**, inset). Data are mean ± s.e.m. $^*P < 0.05$, $^{**}P < 0.01$, $^{***}P < 0.001$, $^{****}P < 0.0001$, log-rank Mantel–Cox test (**a**, **b**, **i**) and unpaired two-tailed *t*-test (**c**–**h**). See accompanying Source Data.

highly metastatic KPC689 orthotopic tumour setting (Extended Data Fig. 10a–g), reducing Kras^{G12D} expression (Extended Data Fig. 10h), increasing survival (Extended Data Fig. 10i) and limiting metastasis (Extended Data Fig. 10j, k).

Discussion

Mutations in *KRAS* are associated with several cancers such as the pancreas, lung and colon[30,31], and oncogenic *KRAS* mutations and activation of downstream effectors such as MEK, AKT and ERK are sufficient drivers of pancreas cancer[3–5,30,32–35]. A sound rationale for targeting RAS emerged for the treatment of cancer[11,36,37], but RAS has remained largely undruggable[6]. Some efficacy were reported with methodologies developed to target oncogenic *Kras* using siRNA molecules[7,8,10,11], but these approaches may have been limited by a lack of specificity and inefficient delivery. Nonetheless, a recent clinical study demonstrated that the polymeric implant *siG12D-LODER*^{TM} was well-tolerated and showed potential efficacy in patients with locally advanced pancreatic cancer[38]. We report that engineered iExosomes can control advanced PDAC in mice and that this approach is clinically feasible[39].

Our studies suggest that exosomes exhibit a superior ability to deliver RNAi and suppress tumour growth when compared to liposomes. Unlike liposomes, the plasma membrane-like phospholipids and membrane-anchored proteins of exosomes may contribute to their diminished clearance from the circulation[12,40,41]. Our results support that the presence of CD47 on exosomes allows for evasion from phagocytosis by the circulating monocytes and increases exosomes half-life in the circulation. Although CD47 does not have a significant role in the entry of exosomes into pancreatic cells, enhanced macropinocytosis in Kras-mutant cancer cells[22,31] favoured their exosomes uptake. Our results also support an efficient uptake of iExosomes despite the stroma-dense features of pancreatic tumours. Whether exosomes entering

cells via this mechanism (macropinocytosis) protect themselves from lysosome-dependent degradation of their content needs further exploration. Collectively, our study offers insight into the therapeutic potential of exosomes in specific targeting of oncogenic *KRAS* in pancreatic cancer.

Online Content Methods, along with any additional Extended Data display items and Source Data, are available in the online version of the paper; references unique to these sections appear only in the online paper.

Received 20 September 2016; accepted 3 April 2017.
Published online 7 June 2017.

1. Hidalgo, M. & Von Hoff, D. D. Translational therapeutic opportunities in ductal adenocarcinoma of the pancreas. *Clin. Cancer Res.* **18,** 4249–4256 (2012).
2. Chang, D. K., Grimmond, S. M. & Biankin, A. V. Pancreatic cancer genomics. *Curr. Opin. Genet. Dev.* **24,** 74–81 (2014).
3. Collins, M. A. *et al.* Oncogenic Kras is required for both the initiation and maintenance of pancreatic cancer in mice. *J. Clin. Invest.* **122,** 639–653 (2012).
4. Collins, M. A. *et al.* Metastatic pancreatic cancer is dependent on oncogenic Kras in mice. *PLoS One* **7,** e49707 (2012).
5. Ying, H. *et al.* Oncogenic Kras maintains pancreatic tumors through regulation of anabolic glucose metabolism. *Cell* **149,** 656–670 (2012).
6. Gysin, S., Salt, M., Young, A. & McCormick, F. Therapeutic strategies for targeting Ras proteins. *Genes Cancer* **2,** 359–372 (2011).
7. Pecot, C. V. *et al.* Therapeutic silencing of KRAS using systemically delivered siRNAs. *Mol. Cancer Ther.* **13,** 2876–2885 (2014).
8. Yuan, T. L. *et al.* Development of siRNA payloads to target KRAS-mutant cancer. *Cancer Discov.* **4,** 1182–1197 (2014).
9. Xue, W. *et al.* Small RNA combination therapy for lung cancer. *Proc. Natl Acad. Sci. USA* **111,** E3553–E3561 (2014).
10. Réjiba, S., Wack, S., Aprahamian, M. & Hajri, A. K-ras oncogene silencing strategy reduces tumor growth and enhances gemcitabine chemotherapy efficacy for pancreatic cancer treatment. *Cancer Sci.* **98,** 1128–1136 (2007).
11. Zorde Khvalevsky, E. *et al.* Mutant KRAS is a druggable target for pancreatic cancer. *Proc. Natl Acad. Sci. USA* **110,** 20723–20728 (2013).
12. van der Meel, R. *et al.* Extracellular vesicles as drug delivery systems: Lessons from the liposome field. *J. Control Release* **195,** 72–85 (2014).
13. Kowal, J., Tkach, M. & Théry, C. Biogenesis and secretion of exosomes. *Curr. Opin. Cell Biol.* **29,** 116–125 (2014).
14. Johnsen, K. B. *et al.* A comprehensive overview of exosomes as drug delivery vehicles - endogenous nanocarriers for targeted cancer therapy. *Biochim. Biophys. Acta* **1846,** 75–87 (2014).
15. Vader, P., Mol, E. A., Pasterkamp, G. & Schiffelers, R. M. Extracellular vesicles for drug delivery. *Adv. Drug Deliv. Rev.* **106,** 148–156 (2016).
16. Kaur, S. *et al.* CD47-dependent immunomodulatory and angiogenic activities of extracellular vesicles produced by T cells. *Matrix Biol.* **37,** 49–59 (2014).
17. Kibria, G. *et al.* A rapid, automated surface protein profiling of single circulating exosomes in human blood. *Sci. Rep.* **6,** 36502 (2016).
18. Brown, E. J. & Frazier, W. A. Integrin-associated protein (CD47) and its ligands. *Trends Cell Biol.* **11,** 130–135 (2001).
19. Jaiswal, S. *et al.* CD47 is upregulated on circulating hematopoietic stem cells and leukemia cells to avoid phagocytosis. *Cell* **138,** 271–285 (2009).
20. Chao, M. P., Weissman, I. L. & Majeti, R. The CD47-SIRPα pathway in cancer immune evasion and potential therapeutic implications. *Curr. Opin. Immunol.* **24,** 225–232 (2012).
21. Commisso, C. *et al.* Macropinocytosis of protein is an amino acid supply route in Ras-transformed cells. *Nature* **497,** 633–637 (2013).
22. Simões, S. *et al.* Cationic liposomes for gene delivery. *Expert Opin. Drug Deliv.* **2,** 237–254 (2005).
23. Willingham, S. B. *et al.* The CD47-signal regulatory protein alpha (SIRPα) interaction is a therapeutic target for human solid tumors. *Proc. Natl Acad. Sci. USA* **109,** 6662–6667 (2012).
24. Nakase, I., Kobayashi, N. B., Takatani-Nakase, T. & Yoshida, T. Active macropinocytosis induction by stimulation of epidermal growth factor receptor and oncogenic Ras expression potentiates cellular uptake efficacy of exosomes. *Sci. Rep.* **5,** 10300 (2015).
25. Özdemir, B. C. *et al.* Depletion of carcinoma-associated fibroblasts and fibrosis induces immunosuppression and accelerates pancreas cancer with reduced survival. *Cancer Cell* **25,** 719–734 (2014).
26. Ijichi, H. *et al.* Inhibiting Cxcr2 disrupts tumor-stromal interactions and improves survival in a mouse model of pancreatic ductal adenocarcinoma. *J. Clin. Invest.* **121,** 4106–4117 (2011).
27. Sherman, M. H. *et al.* Vitamin D receptor-mediated stromal reprogramming suppresses pancreatitis and enhances pancreatic cancer therapy. *Cell* **159,** 80–93 (2014).
28. Provenzano, P. P. *et al.* Enzymatic targeting of the stroma ablates physical barriers to treatment of pancreatic ductal adenocarcinoma. *Cancer Cell* **21,** 418–429 (2012).
29. Olive, K. P. *et al.* Inhibition of Hedgehog signaling enhances delivery of chemotherapy in a mouse model of pancreatic cancer. *Science* **324,** 1457–1461 (2009).
30. Guerra, C. & Barbacid, M. Genetically engineered mouse models of pancreatic adenocarcinoma. *Mol. Oncol.* **7,** 232–247 (2013).
31. Ying, H. *et al.* Genetics and biology of pancreatic ductal adenocarcinoma. *Genes Dev.* **30,** 355–385 (2016).
32. Gidekel Friedlander, S. Y. *et al.* Context-dependent transformation of adult pancreatic cells by oncogenic K-Ras. *Cancer Cell* **16,** 379–389 (2009).
33. Pylayeva-Gupta, Y., Lee, K. E., Hajdu, C. H., Miller, G. & Bar-Sagi, D. Oncogenic Kras-induced GM-CSF production promotes the development of pancreatic neoplasia. *Cancer Cell* **21,** 836–847 (2012).
34. Biankin, A. V. *et al.* Pancreatic cancer genomes reveal aberrations in axon guidance pathway genes. *Nature* **491,** 399–405 (2012).
35. Eser, S., Schnieke, A., Schneider, G. & Saur, D. Oncogenic KRAS signalling in pancreatic cancer. *Br. J. Cancer* **111,** 817–822 (2014).
36. Singh, H., Longo, D. L. & Chabner, B. A. Improving prospects for targeting RAS. *J. Clin. Oncol.* **33,** 3650–3659 (2015).
37. Zeitouni, D., Pylayeva-Gupta, Y., Der, C. J. & Bryant, K. L. KRAS mutant pancreatic cancer: no lone path to an effective treatment. *Cancers (Basel)* **8,** E45 (2016).
38. Golan, T. *et al.* RNAi therapy targeting KRAS in combination with chemotherapy for locally advanced pancreatic cancer patients. *Oncotarget* **6,** 24560–24570 (2015).
39. Kordelas, L. *et al.* MSC-derived exosomes: a novel tool to treat therapy-refractory graft-versus-host disease. *Leukemia* **28,** 970–973 (2014).
40. Clayton, A., Harris, C. L., Court, J., Mason, M. D. & Morgan, B. P. Antigen-presenting cell exosomes are protected from complement-mediated lysis by expression of CD55 and CD59. *Eur. J. Immunol.* **33,** 522–531 (2003).
41. Gomes-da-Silva, L. C. *et al.* Lipid-based nanoparticles for siRNA delivery in cancer therapy: paradigms and challenges. *Acc. Chem. Res.* **45,** 1163–1171 (2012).

Supplementary Information is available in the online version of the paper.

Acknowledgements This work was primarily supported by the Cancer Prevention and Research Institute of Texas, the Knowledge Gap funding of MD Anderson Cancer Center, and NCI grant CA213233. Other support include: V.S.L. laboratory: UT MDACC Khalifa Bin Zayed Al Nahya Foundation; High Resolution Electron Microscopy Facility: Institutional Core Grant CA16672; MDACC Flow Cytometry core facility; and J.J.L. laboratory: NIH P30CA16672; MDACC Small Animal Imaging Facility: NIH P30-CA016672 and 5U24-CA126577. The mass spectrometry-related analysis (SAM) was supported by the NORTE-01-0145-FEDER-000029 (NORTE 2020; ERDF) and FEDER funds (POCI-01/0145-FEDER-016618) and FCT-PTDC/BIM-ONC/2754/2014. We thank K. Dunner Jr for the help with the transmission electron microscopy and immunogold techniques, E. Chang for slide scanning, D. Lundy for tissue processing, J. Carstens and C. Kahlert for independent analyses of tissue histopathology, J. Kaye and L. Gibson for mouse husbandry support, C. Kingsley and D. Lundy for MRI support, E. Lawson for IVIS imaging help, and P. Correa-de-Sampaio for microscopy imaging help.

Author Contributions R.K. conceptually designed the experimental strategy, provided intellectual input and helped to write the manuscript. H.S. and V.S.L. injected mice orthotopically with tumour cells. H.S. performed necropsy analyses and quantification of exosomes in pancreas tissue sections. V.S.L. provided intellectual input, extracted RNA and quantified siRNA loading in exosomes by qPCR analyses, stained tissues for Kras, helped with *in vivo* experiments, designed the experimental strategy, prepared figures and wrote the manuscript. S.K. and S.Y. prepared exosomes (cultured cells for exosome collection and preparation by ultracentrifugation), generated iExosomes (electroporation and wash steps involved in the generation of iExosome and NanoSight measurements), and treated mice with iExosomes. S.Y. also performed an independent analysis of *in vivo* imaging data, generated and genotyped KTC and KPC mice for iExosome treatment, and helped prepare the figures. S.K. provided intellectual input, helped design the experimental strategy, and performed experiments, including treatment of mice with iExosomes, preparation of exosomes for sucrose gradient and qPCR analyses. Unless otherwise noted, S.K. performed the independent replication of the experiments. S.K. performed sucrose gradient analyses, NanoSight measurements, flow cytometry experiments and analyses, immunostaining and analyses, RNA extraction and qPCR of treated cells, MTT and TUNEL assays, macropinocytosis and western blot analyses, analysed data, prepared figures, and helped to write the manuscript. S.A.M. advised and provided intellectual input to the siRNA identification experiments, MTT assays, qPCR analyses, western blots for p-ERK, and one PANC-1 tumour study and one KTC *in vivo* experiment. C.F.R. provided the mass spectrometry data and the relevant section in the Methods. J.J.L. reviewed the source data, advised on experimental design, and supervised statistical analyses.

Author Information Reprints and permissions information is available at www.nature.com/reprints. The authors declare competing financial interests: details are available in the online version of the paper. Readers are welcome to comment on the online version of the paper. Publisher's note: Springer Nature remains neutral with regard to jurisdictional claims in published maps and institutional affiliations. Correspondence and requests for materials should be addressed to R.K. (rkalluri@mdanderson.org).

METHODS

Cell culture. Human BJ, Capan-1 and MIA PaCa-2 cells were cultured in DMEM supplemented with 10% exosome-depleted FBS and 1% penicillin–streptomycin. PANC-1, BxPC-3 and T3M4 cells were cultured in RPMI with 10% FBS and 1% penicillin–streptomycin. All cells lines were from American Type Culture Collection (ATCC) except for T3M4 (Cell Bank, RIKEN BioResource Center); there were no additional validation of the cell lines performed. Cells tested negative for mycoplasma. Luciferase-expressing PANC-1 and BxPC-3 cells (expressing a CMV promoter 5′ to the firefly luciferase protein) were gifts from T. Arumugam. The KPC689 cancer cell line was established from the pancreas tumours of *Pdx1*$^{cre/+}$;*LSL-Kras*$^{G12D/+}$;*LSL-Trp53*$^{R172H/+}$ (KPC) mice[42]. KPC689 cells were engineered to stably express GFP and luciferase after infection with F-Luc-GFP lentivirus (Capital Biosciences). C57BL/6 wild-type fibroblasts were isolated from the ears of C57BL/6 mice by mincing the isolated ears in DMEM supplemented with collagenase type 4 (400 U ml^{-1}) and incubating overnight. The next day, cells and tissue pieces were washed with DMEM supplemented with 20% FBS and 1% penicillin–streptomycin and expanded in this media. For exosome collection, cells were cultured using exosome-depleted FBS. The same procedure was performed on the CD47-knockout (B6.129S7-*Cd47*^{tm1Fpl}/J) mice and C57BL/6 mice to generate ear and tail fibroblast lines. For overexpression of CD47 on BJ fibroblasts, transfections were performed using Lipofectamine 2000 reagent (Invitrogen) with pCMV6-AC-GFP CD47 plasmid (Origene, MG204706), after which exosomes were isolated using the standard protocol described below.

Isolation and purification of exosomes. Exosomes were purified by differential centrifugation processes, as described previously[43–46]. Exosome-depleted FBS was prepared as follows: FBS was filtered using a 100-nm filter, then ultracentrifuged for 16 h, and then filtered again using a 100-nm filter. Supernatant was collected from cells that were cultured in media containing exosome-depleted FBS for 48 h, and was subsequently subjected to sequential centrifugation steps at 800*g* for 5 min, and 2,000*g* for 10 min. This resulting supernatant was then filtered using 0.2-μm filters, and a pellet was recovered at 100,000*g* in a SW32 Ti rotor after 2 h of ultracentrifugation (Beckman). The supernatant was aspirated and the pellet was resuspended in PBS and subsequently ultra-centrifuged at 100,000*g* for another 2 h. The purified exosomes were then analysed and used for experimental procedures. For treatment of exosomes with proteinase K, purified exosomes were incubated (37 °C, 30 min) with 5 mg ml^{-1} of proteinase K (Sigma-Aldrich, dissolved in RNase-free water) followed by heat inactivation (60 °C, 20 min). For RNase treatment, purified exosomes were incubated (37 °C, 30 min) with 2 mg ml^{-1} of protease-free RNase A (Thermo Scientific) followed by addition of 10× concentrated RNase inhibitor (Ambion). These exosomes were then subsequently used for FACS analysis, *in vitro* assays and treatment of tumour-bearing mice, as described below.

Sucrose gradient. Sucrose density gradients[47] were performed to characterize the exosomes. For the 'bottom-up' sucrose gradient separation (Extended Data Fig. 1f), the exosomes, resuspended in 2 ml of HEPES/sucrose solution (2.5 M sucrose, 20 mM HEPES/NaOH solution, pH 7.4), were loaded first in the bottom of the tube and overlaid with a 9 ml linear sucrose gradient (2.0–0.25 M sucrose, 20 mM HEPES/NaOH, pH 7.4) in a SW41 tube (Beckman, 11 ml). For the 'top-down' sucrose gradient separation (Extended Data Fig. 1g), exosomes were resuspended in 1 ml HEPES/sucrose solution (0.25 M sucrose, 20 mM HEPES-NaOH, pH 7.4). A 10 ml linear sucrose gradient (2.0–0.25 M sucrose, 20 mM HEPES-NaOH, pH 7.4) was built into a SW41 ultracentrifuge tube, and the exosomes suspension (1 ml, 0.25 M sucrose, 20 mM HEPES-NaOH, pH 7.4) was deposited on top of this linear sucrose gradient. In both types of sucrose gradient experiment (bottom-up and top-down), the gradients were ultracentrifuged for 16 h at 210,000*g* at 4 °C. Gradient fractions of 1 ml were collected from the top to the bottom of the tube, and the densities of each fractions were evaluated using a refractometer. Each layer was placed into a separate centrifuge tube, and PBS was added to a final volume of 11 ml, then this was ultracentrifuged at 150,000*g* at 4 °C for 2 h. The pellets for each layer were resuspended in 200 μl PBS and loaded onto a black 96-welled microplate to detect the AF647 fluorophore-tagged siRNA contained in them using a fluorescence detection plate reader. A microplate containing 200 μl PBS was used for background readings. The detection of the fluorescence of AF647 fluorophore is depicted as the ratio of fluorescent intensity of the sucrose gradient layer wells to the fluorescent intensity of PBS (negative control)-containing wells. The sucrose gradient experiments (both bottom-up and top-down experiments) were also performed with the siKras^{G12D} iLiposomes and electroporated siKras^{G12D} siRNA. A total of three independent experiments were performed and the results from each of these experiments are shown in Extended Data Fig. 1f, g.

Electroporation of exosomes and liposomes. Approximately 10^9 total exosomes (measured by NanoSight analysis) and 1 μg siRNA or plasmid (for shRNA silencing) were mixed in 400 μl electroporation buffer (1.15 mM potassium phosphate pH 7.2, 25 mM potassium chloride, 21% Optiprep). These exosomes were electroporated using a single 4 mm cuvette using a Gene Pulser Xcell Electroporation System (BioRad, 165-2081), as previously described[45,46]. The cuvette electrode plates are made of aluminium that allows for a uniform pulse delivery to the entire system. In brief, after adding 400 μl of RNAi–exosomes mixture to the cuvette, it was electroporated at 400 V, 125 μF and ∞ ohms, and the cuvette was immediately transferred to ice. Of note, when injecting multiple mice or using more than 10^9 exosomes and 1 μg siRNA, a master mix of exosomes and siRNA is prepared in the electroporation buffer, and 400 μl of the mixture is aliquoted into each cuvette before electroporation. A similar procedure was performed using liposomes (100 nm, purchased from Encapsula Nano Sciences). After electroporation, exosomes were washed with PBS, as described above. After the wash, the exosomes are resuspended in PBS, kept on ice and injected into the mice immediately. After this wash step, the mice were dosed with, conservatively, 10^8 iExosomes per injection in 100 μl PBS volume. This dosage represents approximately 0.15–0.20 μg of exosome protein, and mice thus received approximately 0.15–0.20 μg of exosome protein every 48 h. For *in vitro* transfection, exosomes and liposomes were electroporated and washed with PBS as described above, and 200,000 cells in a 6-well plate were treated with exosomes and liposomes for the indicated time as described for each assay and subsequently washed with PBS and used for further analysis. The siRNA sequence (sense strand 5′-GUUGGAGCUGAUGGCGUAGTT-3′, antisense 5′-CUACGCCAUCAGCUCCAACTT-3′) reflects a G-to-A nucleotide deviation from the wild-type *Kras* gene sequence (bold) to specifically target the glycine-to-aspartate amino acid substitution (Kras^{G12D}) and include a TT nucleotide overhang (underlined) to promote silencing efficiency, as described previously[10,48,49]. The central position of the nucleotide deviant in this *Kras*^{G12D} siRNA enhances its specificity against the wild-type mRNA sequence. This was also labelled with an AF647 fluorophore at the 3′ end on the sense strand to track its delivery. The siRNA was obtained from Qiagen (1027424). All Stars Negative siRNA (scrambled siRNA) was obtained from Qiagen (1027287). The siRNA sequences were also tagged with AF647. A second scrambled siRNA control was used (sense strand 5′-UUCUCCGAACGUGUCACGUTT-3′, antisense 5′-ACGUGACACGUUCGGAGAATT-3′; Extended Data Fig. 4g) and the results were consistent with the scrambled siRNA from Qiagen. The *Kras*^{G12D} shRNA sequence used was 5′CCGGGTTGGAGCTGATGGCGTAGTTCTCGAGCTACGCCATCAGCTCCAACTTTTTT-3′, and was flanked with Age1 and EcoR1 sequences to allow for cloning into the pLKO.1 vector, according to the manufacturer's protocol (Addgene). The shRNA sequence reflects a G-to-A nucleotide deviation from the wild-type *Kras* gene sequence (bold) so that to specifically target the glycine-to-aspartate amino acid substitution in the Kras^{G12D} mutation. Scrambled pLKO.1 shRNA was obtained from Addgene. For experiments performed on siRNA electroporated without exosomes, 1 μg siRNA was added to 400 μl electroporation buffer, and electroporated as described above. This mixture was then ultracentrifuged for 2 h at 100,000*g* either by itself, or after it was mixed with 10^9 exosomes (room temperature and 37 °C, in PBS for 30 min), and then used for further downstream assays. Notably, freshly prepared exosomes were used for every single assay reported in this manuscript, in both *in vivo* and *in vitro* experiments.

Immunogold labelling and electron microscopy. Fixed specimens at an optimal concentration were placed onto a 300 mesh carbon/formvar-coated grids and allowed to absorb to the formvar for a minimum of 1 min. For immunogold staining, the grids were placed into a blocking buffer for a block/permeabilization step for 1 h. Without rinsing, the grids were immediately placed into the primary antibody at the appropriate dilution overnight at 4 °C (monoclonal anti-CD9 1:10, Abcam). As controls, some grids were not exposed to the primary antibody. The next day, all of the grids were rinsed with PBS then floated on drops of the appropriate secondary antibody attached with 10 nm gold particles (AURION) for 2 h at room temperature. Grids were rinsed with PBS and placed in 2.5% glutaraldehyde in 0.1 M phosphate buffer for 15 min. After rinsing in PBS and distilled water, the grids were allowed to dry and stained for contrast using uranyl acetate. The samples were viewed with a Tecnai Bio Twin transmission electron microscope (FEI) and images were taken with an AMT CCD Camera (Advanced Microscopy Techniques).

Flow cytometry analyses of exosomes. Exosomes from BJ fibroblasts, BJ fibroblasts overexpressing CD47, CD47-knockout mouse ear fibroblasts and wild-type C57BL/6 mouse ear fibroblasts were isolated as described above and resuspended in 200 μl PBS. Aldehyde sulfate beads (10 μl, Life Technologies) were added to the solution and beads and exosome mixture were allowed to mix using a bench-top rotator for 15 min at room temperature. PBS (600 μl) was then added to the solution and mixing was continued overnight at 4 °C. 1 M glycine (400 μl) was added and mixing was continued for 1 h at room temperature. The mixture was then spun down at 14,000*g* at room temperature for 1 min. The precipitate was then resuspended in 100 μl of 10% BSA in PBS, and mixed for 45 min at room temperature. The mixture was spun down at 12,000 r.p.m. for 1 min at room temperature and

the supernatant aspirated. The beads with the exosomes attached (pellet) were then resuspended in 40 μl of 2% BSA in PBS, and split equally into two tubes: one for staining for CD47, CD63 or CD81, the other for control (secondary antibody only). The exosomes bound to beads were then incubated with 1 μl anti-CD47 antibody (for mouse: BD Biosciences 556045; for human: eBiosciences 14-0479) or 3 μl anti-CD63 (for mouse: Santa Cruz Biotech SC-31211; for human: BD Biosciences 556019) or anti-CD81 antibody (for human: BD Biosciences 555675) in 20 μl volume, and mixed at room temperature for 30 min. The mixture was then centrifuged at 12,000 r.p.m. for 1 min at room temperature, the supernatant aspirated, and the pellet resuspended in 20 μl of 2% BSA in PBS. Secondary antibodies were then added and the samples were mixed at room temperature for 1 h. The samples were then centrifuged at 12,000 r.p.m. for 1 min at room temperature, supernatant was aspirated, and pellet was resuspended in 200 μl of 2% BSA in PBS. The exosomes bound to the beads were washed three times with 2% BSA in PBS. CD47, CD63 and CD81 detection on the beads was analysed using the LSR Fortessa X-20 cell analyser. All control samples were run alongside experimental samples.

Flow cytometry analysis for exosomes and liposomes biodistribution. Exosomes and liposomes were labelled with PKH67 (Sigma Aldrich) according to the manufacturer's protocol. Alternatively, the exosomes and liposomes were electroporated with AF647-tagged siRNA before injection in mice. These were then injected intraperitoneally into C57BL/6 or nude mice. Plasma was then obtained from these mice at the listed time points after injection of either exosomes or liposomes. The plasma was then diluted in 11 ml PBS and filtered through a 0.2-μm pore filter. Subsequently, the samples were then ultracentrifuged overnight at 150,000*g* at 4 °C. The pellet was then washed with PBS, and followed by a second step of ultracentrifugation at 150,000*g* for 2 h at 4 °C. The samples were then resuspended in 200 μl PBS. Aldehyde sulfate beads (10 μl, Life Technologies) were added to the solution and the beads and exosomes/liposomes mixture was allowed to mix using a bench-top rotator for 15 min at room temperature. PBS (600 μl) was then added to the solution and mixing was continued overnight at 4 °C. 1 M glycine (400 μl) was added and mixing was continued for 1 h at room temperature. The mixture was then spun down at 14,000*g* at room temperature for 1 min, supernatant aspirated, and pellet resuspended in 200 μl of 2% BSA in PBS. The exosomes/liposomes bound to the beads were washed three times with 2% BSA in PBS. FITC or allophycocyanin (APC)-positive beads were analysed using the LSR Fortessa X-20 cell analyser. All control samples were run alongside experimental samples.

Flow cytometry analysis for binding efficiency of CD47-neutralizing antibody on exosomes. Exosomes from BJ fibroblasts were isolated as described above, and then incubated with 10 μg ml^{-1} of anti-CD47 neutralizing monoclonal antibody (Bio-Xcell, B6H12 or 2D3 clones, as specified) for 1 h at either room temperature or 37 °C, or overnight at 4 °C, and then bound to aldehyde sulfate beads as described above. 1 M glycine (400 μl) was added and mixing was continued for 1 h at room temperature. The mixture was then spun down at 12,000 r.p.m. at room temperature for 1 min. The samples were washed with 2% BSA, and secondary antibody (Alexa Fluor 488) was then added and the samples were mixed at room temperature for 1 h. The samples were then centrifuged at 12,000 r.p.m. for 1 min at room temperature, supernatant aspirated, and pellet resuspended in 200 μl of 2% BSA in PBS. The exosomes bound to the beads were washed three times with 2% BSA in PBS. Alexa Fluor 488-positive beads were then analysed using the LSR Fortessa X-20 cell analyser. All control samples were run alongside experimental samples.

Flow cytometry analysis for comparison of binding efficiency of exosomes and liposomes to aldehyde sulfate beads. Exosomes and liposomes were electroporated with AF647-tagged siRNA as described above. The samples were then resuspended in 200 μl of PBS. Aldehyde sulfate beads (10 μl, Life Technologies) were added to the solution and the beads and exosomes/liposomes mixture was allowed to mix using a bench-top rotator for 15 min at room temperature. PBS (600 μl) was then added to the solution and mixing was continued overnight at 4 °C. 1 M glycine (400 μl) was added and mixing was continued for 1 h at room temperature. The mixture was then spun down at 12,000 r.p.m. at room temperature for 1 min, supernatant aspirated, and pellet resuspended in 200 μl of 2% BSA in PBS. The exosomes/liposomes bound to the beads were washed three times with 2% BSA in PBS. AF647$^+$ beads were analysed using the LSR Fortessa X-20 cell analyser. All control samples were run alongside experimental samples.

Visualization of exosomes biodistribution in the tissue. Exosomes were labelled with PKH67 (Sigma Aldrich) according to the manufacturer's protocol. Alternatively, the exosomes were electroporated with AF647-tagged siRNA before injection in mice. These were then injected intraperitoneally into C57BL/6 mice. The specific organs were obtained from these mice at the listed times after injection and then were frozen. Sectioned tissue was stained with DAPI nuclear stain, and images were then captured using Zeiss Observer Z1 inverted microscope. Images were quantified by counting the number of nuclei that had PKH67-labelled/AF647-labelled exosomes surrounding it (PKH67/AF647-positive cells) and divided by the total number of nuclei, in five random visual fields per organ (magnification, ×400). For evaluation of the entry of exosomes in the various pancreas structures, exosomes electroporated with AF647-tagged siRNA were injected intraperitoneally into 26-day-old KTC mice. The pancreas of these mice was then collected 24 h later, mounted in OCT compound and frozen. Sectioned tissue was stained with DAPI nuclear stain, and the images were then captured using Zeiss Observer Z1 inverted microscope. Images were quantified by counting the number of nuclei within a particular structure (islet, acinus, duct, cancer-associated fibroblast, tumour) that had AF647-labelled exosomes surrounding it (AF647$^+$ cells) and dividing by the total number of nuclei within that structure (400×). All control samples were run alongside experimental samples.

Quantitative PCR analyses. Cells were incubated with iExosomes for 3 h, after which RNA was retro-transcribed with MultiScribe Reverse Transcriptase (Applied Biosystems) and oligo-d(T) primers following total RNA purification with Trizol (Invitrogen), according to the manufacturer's directions. Quantitative PCR (qPCR) analyses were performed on an ABI PRISM 7300HT Sequence Detection System Instrument using SYBR Green Master Mix (Applied Biosystems). The transcripts of interest were normalized to 18S transcript levels. Primers for *Kras*^{G12D} were designed as described in ref. 50; *Kras*$^{G12C/V}$ were designed as described in ref. 43; and *Kras* wild-type primers were designed as described in ref. 51. Each reaction included three technical replicates, which were averaged to define one biological replicate. The experiments were repeated three times on distinct days and each experiment defined a biological replicate. Statistical analyses were performed on ΔC_t of biological replicates (mice or independent experiments) and the results expressed as relative fold change. Primer sequences were as follows: human *KRAS*^{G12D}: forward 5′-ACTTGTGGTAGTTGGAGCAGA-3′, reverse 5′-TTGGATCATATTCGTCCACAA-3′. Mouse *Kras*^{G12D} : forward 5′-ACTTGTGGTGGTTGGAGCAGC-3′, reverse 5′-TAGGGTCATACTCATCCACAA-3′. Human wild-type *KRAS*: forward 5′-ATTGTGAATGTTGGTGT-3′, reverse 5′-GAAGGTCTCAACTGAAATT-3′. 18S: forward 5′-GTAACCCGTTGAACCCCATT-3′, reverse 5′-CCATCCAATCGGTAGTAGCG-3′. Human *KRAS*^{G12V}: forward 5′-ACTTGTGGTAGTTGGAGCAGT-3′, reverse 5′-TTGGATCATATTCGTCCACAA-3′. Human *KRAS*^{G12C}: forward 5′-AACTTGTGGTAGTTGGAGATT-3′, reverse 5′-TTGGATCATATTCGTCCACAA-3′.

In some experiments, before the treatment of PANC-1 cells, the exosomes were subjected to a variety of treatments, as follows. siKras^{G12D} iExo: PANC-1 cells were treated with siKras^{G12D} iExo (BJ-derived exosomes). Media Exo: FBS-depleted culture medium was incubated without cells for 48 h at 37 °C, and then processed to collect exosomes. The ultracentrifuged pellet was electroporated with siKras^{G12D} iExo as performed in the siKras^{G12D} iExo group. siRNA: PANC-1 cells were treated with siKras^{G12D} siRNA (no exosomes, no electroporation). siRNA (E): PANC-1 cells were treated with siKras^{G12D} siRNA that was electroporated ('E'). Exo (E): PANC-1 cells treated with just BJ-derived exosomes were electroporated without siKras^{G12D}. siRNA + Exo: PANC-1 cells were treated with BJ-derived exosomes and siKras^{G12D} was added to the wells of cells concurrently. siRNA (E) + Exo: PANC-1 cells were treated with BJ-derived exosomes that were mixed with electroporated siKras^{G12D}. siRNA + Exo (E): PANC-1 cells were treated with electroporated BJ-derived exosomes that were mixed with siKras^{G12D}. siRNA (E) + Exo (E): PANC-1 cells were treated with electroporated BJ-derived exosomes that were mixed with electroporated siKras^{G12D}. Scramble iExo: PANC-1 cells were treated with BJ-derived exosomes that were electroporated with scrambled siRNA (from Qiagen, as described above). Scramble (2) iExo: PANC-1 cells treated with BJ-derived exosomes that were electroporated with a distinct scrambled siRNA (target sequence: 5′-AATTCTCCGAACGTGTCACGT-3′). All control samples were run alongside experimental samples.

MTT, TUNEL and flow cytometry apoptosis assay. PANC-1, BxPC-3, Capan-1 and MIA PaCa-2 cells were seeded in a 96-well plates (1,000 cells per well) and allowed to seed for 24 h, after which they were treated with exosomes electroporated with *Kras*^{G12D} siRNA, *Kras*^{G12D} shRNA, scrambled siRNA, scrambled shRNA, PBS or non-electroporated control exosomes. Treatment was given only once at the beginning, after seeding of cells. Subsequently, every 24 h, MTT reagent (tetrazole, Sigma Aldrich) was added to the cell culture media for 3 h at 37 °C. The supernatant was then discarded, cells washed with PBS, and lysed with DMSO to dissolve the formazan product. Absorbance was measured at an optical density of 562 nm in a spectrophotometric plate reader. In these MTT experiments, each treatment (for example, iExosomes) was aliquoted into five partitions, and each partition was used to treat three wells of cells. The triplicate wells were averaged to define $n = 1$ partition and each treatment thus totalled $n = 5$ partitions. The MTT assay for PANC-1 and BXPC-3 cells was repeated again under the same conditions, as an independent experiment (Extended Data Fig. 4). For TUNEL assays, cells were treated with iExosomes for 24 h, and apoptosis was assessed using the *In situ* Cell Death Kit, TMR red (Roche), according to the manufacturer's directions. The cells

were fixed with 4% paraformaldehyde (PFA) at room temperature for 20 min, and SYTOX green nucleic acid stain (Invitrogen, 1:10,000 in PBS for 10 min at room temperature) or DAPI was used to delineate the nuclei. Images were taken with a Zeiss LSM 510 confocal microscope, quantified by counting the number of cells with TUNEL positivity per visual field (400×), and results were expressed as the percentage of cells with a positive label out of the total number of cells counted per visual field. The TUNEL assay was repeated again under the same conditions, as an independent experiment (Extended Data Fig. 4). For flow cytometry analysis of apoptosis, PANC-1 cells were treated with iExosomes or scrambled iExosomes for 24 h, and apoptosis and dead cells were measured by LIVE/DEAD fixable aqua (ThermoFisher, L34957) and propidium iodide (5 μl of a 50 μg ml^{-1} stock solution per reaction; from BD Biosciences, 556547), according to the manufacturer's instructions. This was then analysed using the LSR Fortessa X-20 cell analyser. All control samples were run alongside experimental samples.

Visualization and quantification of AF647/CM-DiI in cells treated with exosomes or liposomes. Exosomes isolated from BJ fibroblasts, CD47-knockout fibroblasts, and wild-type C57BL/6 fibroblasts were electroporated with AF647-tagged siRNA and treated with PBS, proteinase K, or trypsin (Life Technologies, 10×, 15 min at room temperature and ultracentrifuged with PBS for 2 h at 4 °C), were washed with PBS for 2 h, and then added to PANC-1 cells cultures on glass coverslips for 3 h. For staining of exosomes with CM-DiI dye (ThermoFisher), isolated exosomes were resuspended in 1 ml PBS, and 2 μl (1:500) of CM-DiI dye was added, after which the mixture was incubated at 37 °C for 5 min, and then at 4 °C for 10 min. This was then ultracentrifuged with PBS for 2 h, and then added to PANC-1 and BxPC-3 cells on glass coverslips for 3 h. The cells were then fixed by washing with cold PBS and incubating with 4% PFA at room temperature for 20 min. The cells were then washed with PBS, incubated with 0.05% Triton X-100 for 10 min, washed with PBS and stained with SYTOX green nuclear stain (Invitrogen) or DAPI. The coverslips were then mounted on to glass slides with mounting media. Accumulation of AF647 or CM-DiI was visualized using Zeiss Observer Z1 inverted microscope. The number of cells with AF647- or CM-DiI-positive labels was counted per visual field (×400), and the results were expressed as the percentage of cells with a positive label out of the total number of cells counted per visual field. All control samples were run alongside experimental samples.

Quantification of loading efficiency within exosomes/liposomes by RT–PCR. A total of 10^9 exosomes or liposomes were electroporated with 1 μg siRNA as described above. When stated, the electroporated exosomes/liposomes were treated with proteinase K and RNase A. Specifically, when both treatments were required, they were performed sequentially. The samples were first treated with proteinase K, the proteinase K was inactivated, and the samples were then washed with PBS and spun down using ultracentrifugation. The resuspended, proteinase K-treated exosomes were then treated with RNase A, the RNase was inactivated, and the exosomes were then washed with PBS and spun down using ultracentrifugation. We also treated exosomes with 1% Triton X-100 before RNase A treatment. In brief, exosomes were subjected to treatment with 1% Triton X-100 for 30 min at 37 °C, after which RNase A was added. siRNA (1 μg) was used as input, and siRNA (1 μg) was also used for RNase A treatment following an identical procedure as listed above. Control exosomes were non-electroporated exosomes. All samples were mixed with 500 μl TRIzol reagent, and 200 μl chloroform was added to the mixtures. The aqueous phase was recovered following 15 min of centrifugation at 10,000*g* at 4 °C. The aqueous phase, 200 μl for each sample, was then mixed with 250 μl of 100% ethanol and bound to filters provided in the Total Exosomes RNA and Protein Isolation Kit (Invitrogen, 4478545). The protocol to purify the RNA was then followed according to the manufacturer's directions. A total of 100 μl of eluted RNA for each sample was obtained. The Custom TaqMan Small RNA Assay kit was purchased (Applied Biosystems) to specifically detect the sense strand of the $Kras^{G12D}$ siRNA and the manufacturer's protocol was followed, using 5 μl RNA template for the reverse transcription reaction, and 1.33 μl of 1:1,000-diluted reverse transcription reaction product for the qPCR. The reactions were also performed by diluting the electroporated exosomes 1:1,000 before proceeding with the described treatments, in which case the reverse transcription reaction product was not diluted. The RNA was extracted as described, reverse transcription reaction performed as described, and 1.33 μl of the reverse transcription reaction product was used for the qPCR. qPCR reactions were run with technical duplicates. The reverse transcription reaction product of the siRNA input sample was also further diluted 1:2 and 1:4 to establish a standard curve. A no-template control was included in the qPCR reaction and this showed no detectable signal. Each exosome and liposome samples was prepared in triplicate, consisting of three independent preparations of exosomes/liposomes electroporation. The mean $1/C_t$ and standard deviation of the three independent experiments are shown. All control samples were run alongside experimental samples.

Protein identification by nano-liquid chromatography coupled to tandem mass spectrometry (LC–MS/MS) analysis. Exosome extraction was performed by ultracentrifugation (Beckman Optima XE 100) at 100,000*g* overnight at 4 °C, followed by two washing steps with 0.9% NaCl (saline). Protein extraction was done using a solution of 8 M urea and 2.5% SDS (Sigma), cOmplete protease inhibitor cocktail (Roche) and phenylmethylsulfonyl fluoride (Sigma), for 30 min on ice followed by centrifugation at 17,000*g* for 30 min. Proteins were present in the supernatant. T3M4 $CD24^+CD44^+$-derived exosome protein was precipitated using methanol/chloroform methodology and quantified with Pierce 660 nm protein assay. A total of 40 μg of protein was used for the analysis. The sample digestion was performed overnight using trypsin solution. The digestion product was purified with SEP-PAK C18 cartridge. For the analysis, 1 μg of peptides were subjected to nano-liquid chromatography (Eksigent Technologies nanoLC Ultra 1D plus, AB SCIEX) coupled to high-speed Triple TOF 5600 mass spectrometer (AB SCIEX) with a Nanospray III source (1 technical replicate). The mass spectrometry data obtained were analysed using Mascot Server v.2.5.0 (Matrix Science) as the search engine against the *Homo sapiens* database (including also the decoy database). The confidence interval for protein identification was set to ≥95% ($P < 0.05$), and only peptides with an individual ion score above the 1% false discovery rate threshold were considered correctly identified.

Western blot. To deduce the protein levels in cell lysates after 24 h of treatment with exosomes, PANC-1 cells were homogenized in RIPA lysis buffer and protein lysates were normalized using Bicinchoninic Acid (BCA) protein assay kit (Pierce, Thermo Fisher Scientific). Protein lysates (20 μg) were loaded onto acrylamide gels for electrophoretic separation of proteins under denaturing conditions and transferred onto PVDF membranes (ImmobilonP) by wet electrophoretic transfer. The membranes were then blocked for 1 h at room temperature with 5% non-fat dry milk in PBS with 0.05% Tween-20, and incubated overnight at 4 °C with the following primary antibodies: anti-rabbit p-ERK-p44/p42 MAPK (ERK1/2) (Thr202/Tyr 204) (Cell Signaling, 4376, 1:1,000) and anti-rabbit vinculin (Abcam, 129002, 1:10,000). Secondary antibodies were incubated for 1 h at room temperature. Washes after antibody incubations were done with an orbital shaker, three times at 15-min intervals, with PBS containing 0.05% Tween-20. Membranes were developed with chemiluminescent reagents from Pierce, according to the manufacturer's instructions. Supplementary Fig. 1 shows uncropped western blots from data presented in Extended Data Fig. 4h. The quantifications were performed on two independent experiments ($n = 2$) with uncropped western blots shown in Supplementary Fig. 1. Western blots were quantified by ImageJ software, in which the p-ERK peak intensity values (selecting both bands that represent p-ERK1 and p-ERK2) were normalized to those of vinculin (selecting the 124-kDa band), in each blot. All control samples were run alongside experimental samples.

RAS binding assay. Lysates from cells treated with iExosomes and controls were isolated according to the manufacturer's instructions (Cytoskeleton, BK008), and subsequently the GTP-bound versus GDP-bound RAS activity in PANC-1 and BxPC-3 cells was measured using the RAS pull-down activation assay kit (Cytoskeleton, BK008), and using western blotting as the final readout. The scanned film saturation was uniformly set to 0 using the format picture tool in PowerPoint and the cropped blots are shown in Extended Data Fig. 4i; and the uncropped, unmodified western blots are shown Supplementary Fig. 1. All control samples were run alongside experimental samples.

Mice. Female athymic *nu/nu* mice (Charles Rivers) between 4 and 6 weeks of age were housed in individually ventilated cages on a 12 h light:12 h dark cycle at 21–23°C and 40–60% humidity. Mice were allowed free access to an irradiated diet and sterilized water. Under general anaesthesia, PANC-1, BxPC-3 (10^6 cells in 10 μl PBS) or KPC689 (5×10^5 cells in PBS) cells were injected into the tail of the pancreas using a 27-gauge syringe. For detection of luciferase expression, the mice were injected intraperitoneally with 100 mg kg^{-1} of body weight of luciferin (200 μl of 10 mg ml^{-1} luciferin in PBS) 12–15 min before imaging, anaesthetized with isoflurane, and imaged using IVIS (Xenogen Spectrum). For tumour burden analyses, Living Image version 4.4 (Caliper Life Sciences) was used to quantify all tumours. A circular region of interest (ROI) around the pancreas and tumour was set within the same experimental groups. In addition, exposure conditions (time, aperture, stage position and binning) were kept identical for all measurements within each experiment.

Tumour measurements for average radiance (photons s^{-1} cm^{-2} sr^{-1}) or total flux (wherever mentioned, photons s^{-1}) were obtained under the same conditions for all experimental groups. All IVIS imaging analyses were ascertained by two independent experimentalists, one of which was blinded to the treatment groups. The mice were imaged regularly and randomly divided into groups for treatments. The mice were monitored daily for signs of distress, and two of the three experimentalists monitoring health status were blinded to the treatment groups. Mice received 10^8 exosomes or liposomes intraperitoneally in 100 μl of PBS

every other day. Exosomes or liposomes were electroporated with 1 μg of siRNA (AF647-tagged siRNA), or shRNA, or were pre-treated with proteinase K and/or RNase A as described above, or were mixed with electroporated siRNA (at room temperature and 37 °C), and washed with PBS before injection.

When using KTC (*Ptf1a*$^{cre/+}$;*LSL-Kras*$^{G12D/+}$;*Tgfbr2*$^{lox/lox}$)[25] genetically engineered mice, exosome treatment was initiated at 18 (early) or 33 (late) days of age. For exosome biodistribution studies, adult C57BL/6 mice were injected intraperitoneally with exosomes labelled with PKH67 (Sigma) or exosomes electroporated with AF647. For the KPC689 orthotopic study, 5×10^5 KPC689 cells were injected orthotopically in the tail of the pancreas of adult female C57BL/6 mice (Jackson Laboratory). These mice were then imaged by IVIS or by MRI 20 days after tumour cell induction. Treatment with exosomes (siKras^{G12D} iExo and siScramble iExo) was started on days 16 (early) and 32 (late) after tumour cell induction, and continued every other day. Another MRI was performed 48 days after tumour cell induction. MRI was performed and analysed as previously described[42]. For experiments aimed to neutralize CD47, 10 μg ml^{-1} anti-CD47 neutralizing monoclonal antibody (Bio-Xcell, B6H12 or 2D3 clones, as specified) was incubated with exosomes or liposomes for 1 h at room temperature, washed with PBS by ultracentrifugation as described above, and injected into the mice. Treatment with both anti-CD47 monoclonal antibody and iExosomes/iLiposomes along with controls was performed every other day. Treatment of KPC mice started when the mice reached 100 days of age. Owing to the variability of the model, the mice were subjected to MRI before treatment start, to determine baseline tumour size, and subsequently grouped into siKras^{G12D} or siScrbl iExosome groups. For gemcitabine studies, a 50 mg kg^{-1} dosage, administered every 48 h intraperitoneally, was used.

At the time of necropsy or euthanasia, gross observation of the metastatic burden and measure of primary tumour burden was performed in a blinded fashion: the experimentalist performing the tissue collection, recording of disease burden and metastasis, was blinded to the treatment group. Blood urea nitrogen, aspartate transaminase and alanine transaminase analyses were performed using plasma (collected using heparin) and BioAssay Systems blood chemistry assay kits (catalogue numbers DIUR-100, EASTR-100 and EALT-100, respectively), following the manufacturer's specifications. In all orthotopic mouse models (PANC-1, BxPC-3 and KPC689), control groups were treated alongside the experimental groups. For KTC and KPC genetically engineered mouse models, mice were enrolled randomly into control or experimental treatment groups when they became available and reached the stated age for treatment start; however, care was taken to ensure, whenever possible, that mice were enrolled into both control and experimental groups together. For KPC mice, baseline MRI confirmed the presence of tumour, after which mice were enrolled into either control or experimental groups at 100 days of age, and control and experimental treatment were administered together when the treatment windows overlapped during the experiment. All animal procedures were reviewed and approved by the Institute for Animal Care and Use Committee at UT MDACC.

Histological analyses. Tissues were fixed in formalin and processed for paraffin embedding. Tissue sections of 5-μm thickness were cut and stained for H&E and MTS (Leica). For histopathological scoring, H&E-stained slides were scored based on the morphological stages of pancreatic cancer: normal, PanIN and PDAC. For each tissue section, a percentage score for each of the three stages were performed in a blinded fashion. Specifically, at least two (three in some experiments) experimentalists evaluated the slides. They each performed their analyses independently from one another, and one of the two, or two of the three, experimentalists were blinded to the treatment groups. All three experimentalists returned identical conclusions and the scores were averaged for each stage of each mouse. Note that while small foci of cancer cells can be seen in the shKras^{G12D} iExo-treated pancreas, the vast majority of the pancreas was histologically unremarkable. For the analysis of fibrosis in mice, six 200× visual fields were randomly selected for each MTS-stained pancreas section, and fibrosis was quantified using a grid intersection analysis with Adobe Photoshop. For each image evaluated, a grid of a 100 squares was overlapped on each picture, and each intersection was counted for blue (fibrotic area) and purple/red (non-fibrotic area). A percentage score was then obtained for each tissue section. Tissue sections were also subjected to antigen retrieval (15 min in 10 nM citrate buffer at pH 6 and 98 °C) before immunostaining. The tissue sections were incubated with 4% CWFS gelatin (Aurion) in either TBS or PBS, 1 h before overnight incubation with the primary antibodies. The following primary antibodies were used for staining: anti-rabbit p-ERK p44/p42 MAPK (ERK1/2) (Thr202/Tyr 204) (immunohistochemistry, Cell Signaling 4376; 1:400), anti-rabbit AKT1 (phospho S473) (immunohistochemistry, Abcam ab81283; 1:100), anti-rabbit Ki-67 (immunohistochemistry, Thermo Scientific RM-9106-S; 1:400) and conjugated anti-actin α-SMA-Cy3 (immunofluorescence, Sigma C6198; 1:100). For co-staining of CK19 and p-ERK, the primary antibodies used were anti-rabbit CK19 (immunofluorescence, Abcam 52625) and anti-rabbit p-ERK p44/p42 MAPK (ERK1/2) (immunofluorescence, Cell Signaling 4370). For immunohistochemistry, the sections were incubated with biotinylated goat anti-rabbit and streptavidin horseradish peroxidase (HRP) (Biocare Medical), for 10 min each, and counterstained with haematoxylin. DAB-positivity was analysed. Note that the quantification was performed on measurably smaller tumour areas in the siKras^{G12D} iExo-treated group compared to large tumour area in the control group. This was performed on at least five, and up to eight 200× pictures per tissue section, and an average of relative percentage positive score was obtained for each tissue section. Ki-67 staining was quantified by counting the number of positively stained nuclei, per visual field (400×), whereas p-ERK, p-AKT and α-SMA staining was quantified with ImageJ to define a positively stained area, which was then expressed as a percentage of the positively stained area to the total image area. Quantification of CK19 and p-ERK co-immunolabelling was performed on eight random 400× images per tissue section, and inserted into FIJI by Image J co-localization software. The TUNEL assay was performed using the *In Situ* Cell Death Detection Kit, TMR red (Roche), according to the manufacturer's directions. AF647 was detected on frozen tissue sections by staining the nuclei with SYTOX green (1:10,000 in PBS for 10 min). Images were taken using a Zeiss LSM 510 confocal microscope, and quantified by counting the number of TUNEL-positive cells per visual field (400×), and results were expressed as the percentage of cells with a positive label out of the total number of cells counted per visual field. PKH67-labelled exosomes or AF647-electroporated exosomes were also injected into mice 3 h before euthanasia, and the pancreases were fixed, processed and sectioned as described above. Sections were mounted on slides, nuclei were stained with DAPI, and the pancreas sections were imaged using the Zeiss Observer Z1 inverted microscope. PKH67/AF647-positive cells were counted in each 400× visual field and differentiated according to tumour or normal peritumoral cells based on nuclear staining characteristics. For the exosome biodistribution studies, the number of PKH67-positive cells was counted in five random 400× visual fields in the brain, gastrointestinal tract, kidney, liver, lung, pancreas and spleen from three mice. The results were expressed as the percentage of cells with a positive label out of the total number of cells counted. For pancreas structure quantification, the number of AF647-positive cells was counted in each 400× visual field in the pancreas, and the results were expressed as the percentage of cells with a positive label out of the total number of cells counted per visual field. Representative pictures of the structures were taken accordingly. For Kras staining in the pancreas tumour, liver, lung, kidney, spleen and heart, 5-μm thick sections from formalin fixed, paraffin-embedded tissues were processed for antigen retrieval (two repeats of 15-min microwave-based antigen retrieval using sodium citrate buffer; 10 mM sodium citrate, 0.05% Tween 20, pH 6.0), then incubated at room temperature for 15 min with 3% H_2O_2 in methanol. The sections were washed in TBS, blocked with Rodent Block M solution (Biocare) for 30–45 min at room temperature, then incubated with a 1:10 dilution of Kras antibody (ThermoFisher, 414700, clone 9.13) in 3% BSA containing PBS diluent, overnight at 4 °C or at room temperature for 4 h. The slides were then processed for secondary antibody application and DAB-based development using Biocare's MACH 4 universal HRP-polymer reagents, according to the manufacturer's recommendation. Analyses for comparative DAB positivity was performed using ImageJ software by designing a macro to define a positively stained area, which was then expressed as a percentage of the positively stained area to the total image area. Each organ had a unique macro programmed for quantification. All control samples were run alongside experimental samples.

Quantification of the number of exosomes from the plasma of mice. CD47-knockout and wild-type C57BL/6 mice were retro-orbitally bled using heparin and the plasma was isolated. Plasma (300 μl per mouse) was then diluted in 11 ml PBS and filtered through a 0.2-μm pore filter. Subsequently, the samples were ultracentrifuged overnight at 150,000*g* at 4 °C. The pellet was then washed with PBS, and followed by a second step of ultracentrifugation at 150,000*g* for 2 h at 4 °C, after which the total number of exosomes in the plasma of the mice was measured by NanoSight analysis. All control samples were run alongside experimental samples.

Macrophage clearance. Immunocompetent C57BL/6 mice between the ages of 10 and 14 weeks were injected intraperitoneally with either exosomes or liposomes containing AF647-tagged siRNA. The blood of these mice was collected 3 h after injection and processed for flow cytometry analyses. Red blood cells were depleted using ACK lysis buffer (Invitrogen), and the peripheral cells were blocked with FC block (1:1,000, BD Pharmingen), stained with Live/Dead Aqua dye (1:200, Life Technologies, 405 nm), anti-CD11b (1:200, BD Pharmingen, PerCP/Cye 5.5) and anti-CD172a (1:200, BD Pharmingen, FITC) antibodies for 30 min, washed with PBS, and analysed using the LSR Fortessa X-20 cell analyser (UT MDACC flow cytometry core facility). Immunocompetent C57BL/6 mice were also intraperitoneally injected with exosomes that were electroporated with AF647-tagged siRNA, and incubated with 10 μg ml^{-1} anti-CD47 neutralizing monoclonal antibody (Bio-Xcell, B6H12 or 2D3 antibodies) for 1 h at room temperature. The blood

of these mice was collected 3 h after injection and processed for flow cytometry analyses as described above. All control samples were run alongside experimental samples.

Macropinosome visualization and quantification. Approximately 50,000 cells (PANC-1 and BxPC-3) were seeded onto glass coverslips, and 24 h after seeding, cells were serum-starved for 18 h. For treatment with EIPA (Sigma Aldrich), cells were pre-treated with 5 μM, 25 μM or 75 μM EIPA for 30 min at 37 °C. DMSO was used as a vehicle. Cells were then incubated with exosomes or liposomes labelled with PKH67 (Sigma Aldrich) for 3 h at 37 °C. Macropinosomes were detected using a high molecular mass tetramethylrhodamine (TMR) dextran (Invitrogen), in which TMR dextran is added to the serum-free media at a concentration of 1 mg ml^{-1} for 30 min at 37 °C. At the end of the incubation period, cells were rinsed five times with cold PBS and fixed with 4% PFA. Cells were then stained with DAPI nuclear stain, and then coverslips were mounted onto the slides. Images were then captured using Zeiss Observer Z1 inverted microscope, and at least three fields from at least three to five separate wells were randomly selected across each sample, and analysed using the 'Analyze Particles' feature on Image J, as described previously[21]. The particle density was then expressed as the relative number of macropinosomes. In brief, the 'macropinocytic index' was computed by determining the total macropinosome area in relation to the total cell area for each field, and then determining the average across all fields. A detailed protocol to analyse and calculate the amount of macropinocytosis within a sample is listed in ref. 21. A similar quantification was performed using the PKH67 label and the result was expressed as the relative number of exosomes or liposomes. The macropinocytosis assay was repeated again as an independent experiment in Extended Data Fig. 7. All control samples were run alongside experimental samples.

Statistical analyses. No statistical methods were used to predetermine sample size. Statistical analyses used are detailed in the figure legends. One-way ANOVA or unpaired two tailed Student's *t*-test was used to establish statistical significance using GraphPad Prism (GraphPad Software). For survival analyses, Kaplan–Meier plots were drawn and statistical differences evaluated using the log-rank (Mantel–Cox) test. $P < 0.05$ was considered statistically significant.

Data availability. Source Data for all figures are provided with the paper, and reagents and all other data are available from the corresponding author upon reasonable request.

42. Zheng, X. *et al.* Epithelial-to-mesenchymal transition is dispensable for metastasis but induces chemoresistance in pancreatic cancer. *Nature* **527,** 525–530 (2015).
43. Melo, S. A. *et al.* Glypican-1 identifies cancer exosomes and detects early pancreatic cancer. *Nature* **523,** 177–182 (2015).
44. Melo, S. A. *et al.* Cancer exosomes perform cell-independent microRNA biogenesis and promote tumorigenesis. *Cancer Cell* **26,** 707–721 (2014).
45. Alvarez-Erviti, L. *et al.* Delivery of siRNA to the mouse brain by systemic injection of targeted exosomes. *Nat. Biotechnol.* **29,** 341–345 (2011).
46. El-Andaloussi, S. *et al.* Exosome-mediated delivery of siRNA *in vitro* and *in vivo*. *Nat. Protocols* **7,** 2112–2126 (2012).
47. Thery, C., Amigorena, S., Raposo, G. & Clayton, A. Isolation and characterization of exosomes from cell culture supernatants and biological fluids. *Curr. Protoc. Cell Biol.* **Chapter 3,** Unit 3.22 (2006).
48. Ma, J. B., Ye, K. & Patel, D. J. Structural basis for overhang-specific small interfering RNA recognition by the PAZ domain. *Nature* **429,** 318–322 (2004).
49. Du, Q., Thonberg, H., Wang, J., Wahlestedt, C. & Liang, Z. A systematic analysis of the silencing effects of an active siRNA at all single-nucleotide mismatched target sites. *Nucleic Acids Res.* **33,** 1671–1677 (2005).
50. Rachagani, S. *et al.* Activated $Kras^{G12D}$ is associated with invasion and metastasis of pancreatic cancer cells through inhibition of E-cadherin. *Br. J. Cancer* **104,** 1038–1048 (2011).
51. Poliseno, L. *et al.* A coding-independent function of gene and pseudogene mRNAs regulates tumour biology. *Nature* **465,** 1033–1038 (2010).

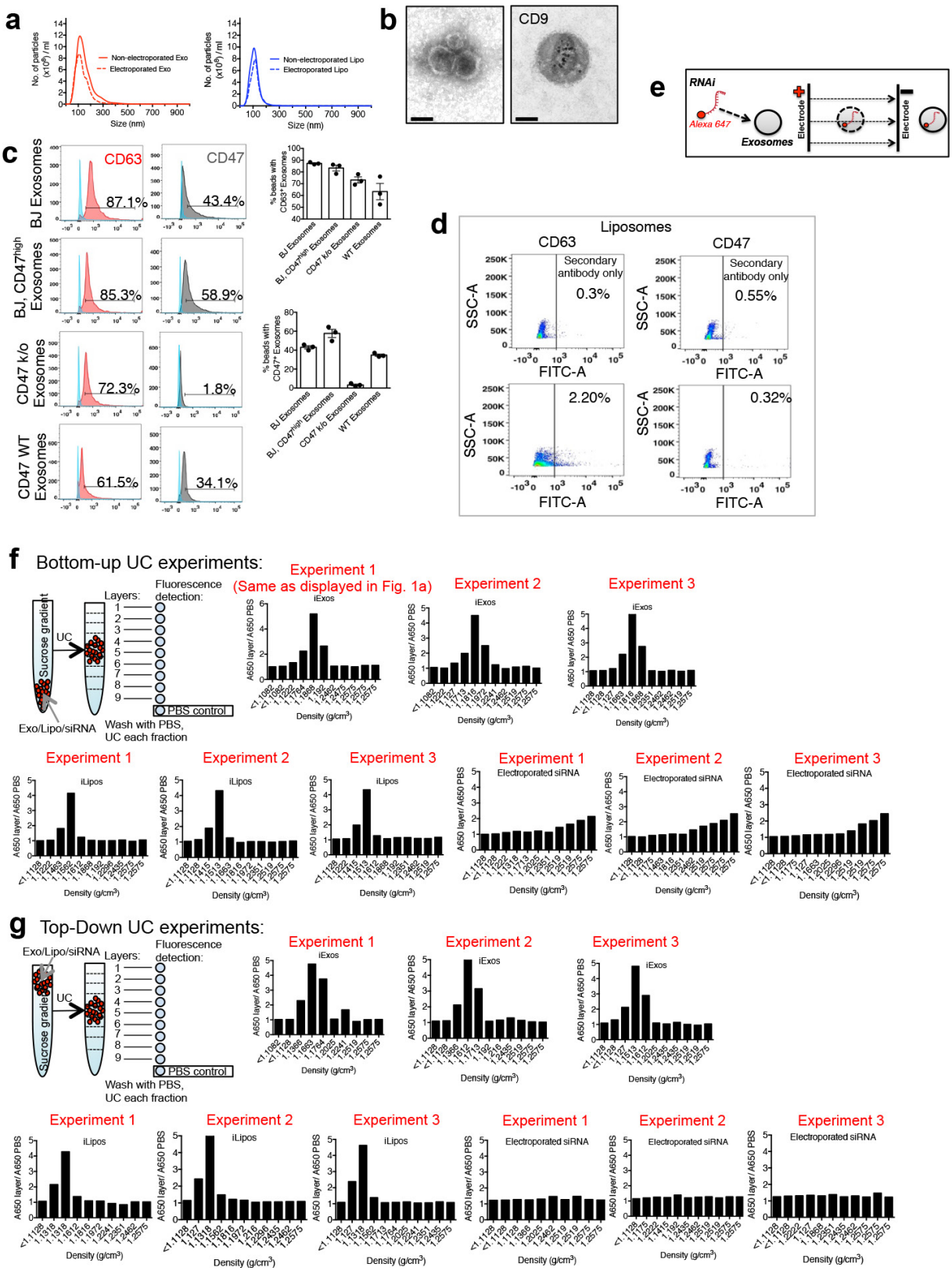

Extended Data Figure 1 | Exosomes purification and siRNA loading. **a**, Exosome and liposome numbers and size distribution using NanoSight analysis. **b**, Transmission electron micrographs of exosomes stained with secondary antibody only (left) or stained for CD9 by immunogold (right). Scale bars, 100 nm. **c**, Flow cytometry analyses of CD63 and CD47 on exosomes. $n = 3$ distinct exosome isolations. **d**, Flow cytometry analyses and quantification of exosomal proteins CD63 and CD47 in liposomes. **e**, Schematic representation of electroporation of RNAi into exosomes. **f**, Schematic (left) and fluorescence intensity plots (right and bottom) of sucrose gradient layers (from the 'bottom-up' method). UC, ultracentrifuge. Results from three independent experiments are shown. **g**, Schematic (left) and fluorescence intensity plots (right and bottom) of sucrose gradient layers (from the 'top-down' method). Results from three independent experiments are shown. Data are mean ± s.e.m. See accompanying Source Data.

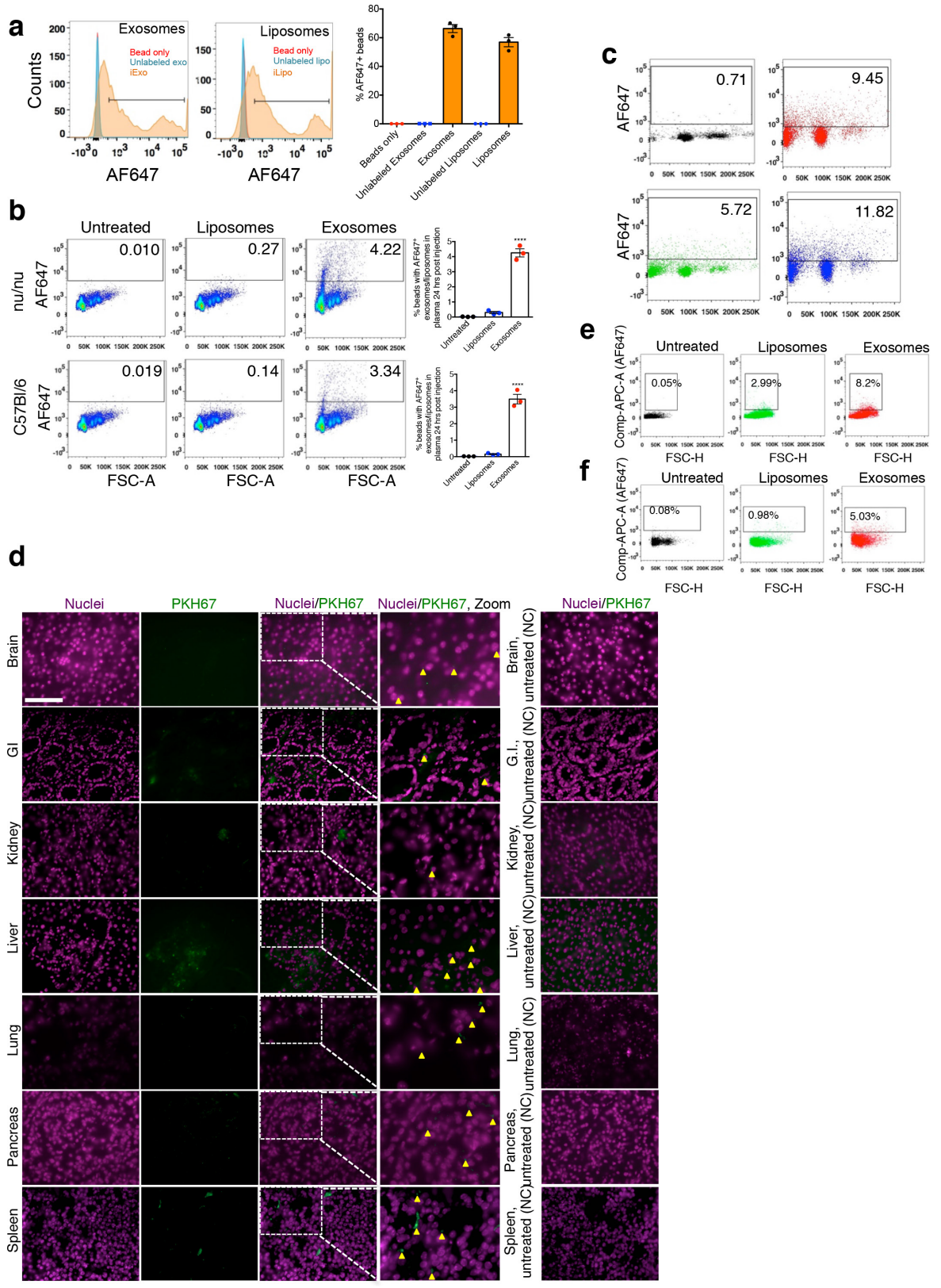

Extended Data Figure 2 | Tissue distribution and clearance of iExosomes. a, Flow cytometry analyses (left) and quantification (right) of the comparison of the binding efficiency to aldehyde sulfate beads. $n = 3$ distinct batches of exosomes and liposomes. **b**, Flow cytometry analyses (left) and quantification (right) of exosomes and liposomes electroporated with AF647-tagged siRNA, isolated from the plasma of C57BL/6 and nude (*nu/nu*) mice, 24 h after injection. $n = 3$ mice per group. **c**, Flow cytometry analyses (from data in Fig. 1b) of exosomes with AF647-tagged siRNA in the circulation of mice. **d**, Representative micrographs of the indicated organs of mice injected intraperitoneally with PKH67-labelled BJ fibroblast exosomes. $n = 3$ mice. Quantification is shown in Fig. 1c. **e**, **f**, Flow cytometry analyses of pancreas cells 6 h (**e**; quantification in Fig. 1d) and 24 h (**f**) after injection of siKras^{G12D} exosomes. Data are mean ± s.e.m. $^{****}P < 0.0001$, one-way ANOVA. See accompanying Source Data.

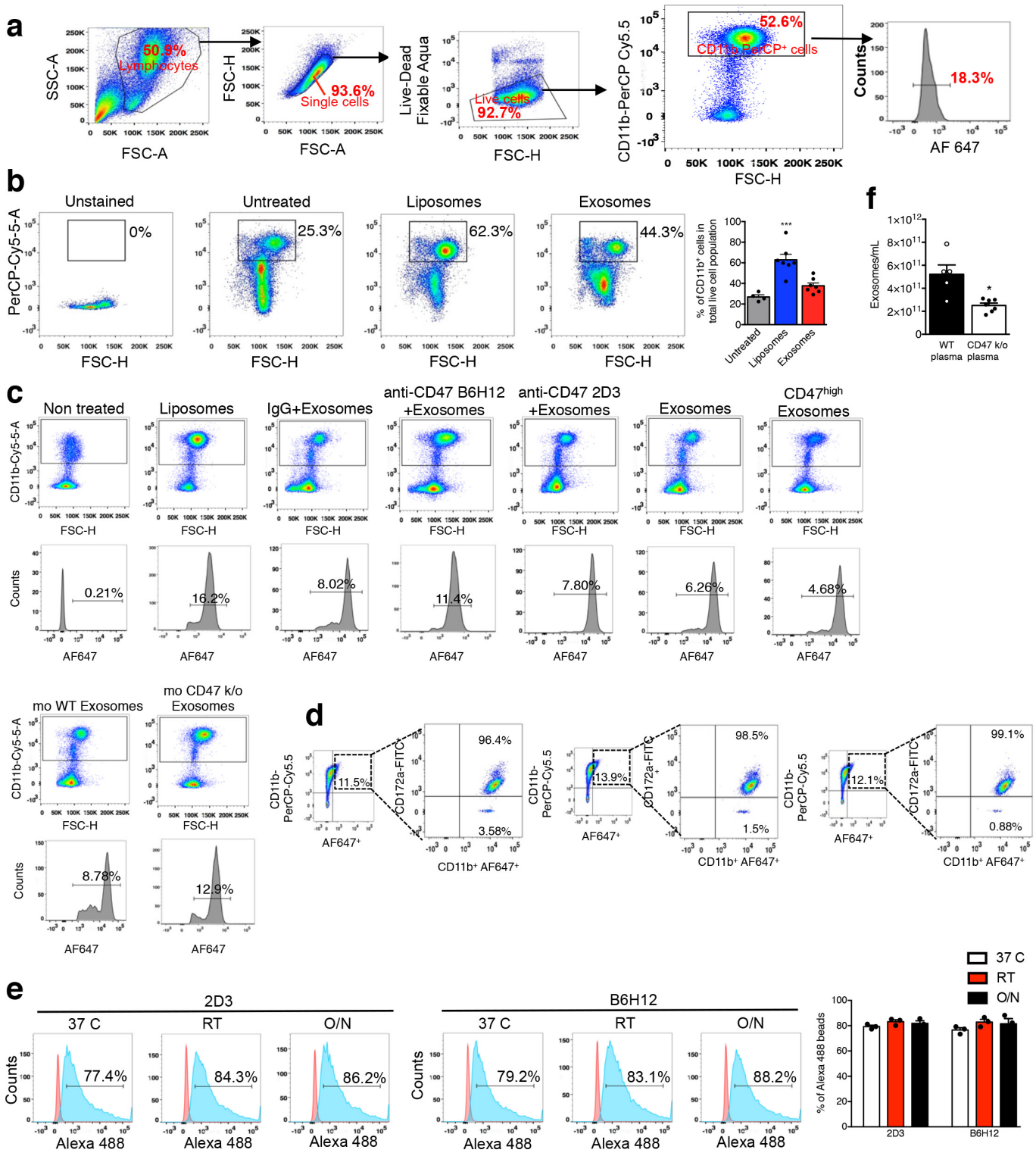

Extended Data Figure 3 | CD47-induced monocyte clearance and iExosome characterization. a, Schematic representation of gating strategy for data in Fig. 1e. **b**, Flow cytometry analysis of $CD11b^+$ cells in the circulation (untreated, $n = 4$ mice), liposomes ($n = 7$ mice) and exosomes ($n = 7$ mice). Unstained sample was used to control for background signal. **c**, Representative dot plots from Fig. 1e. **d**, Flow cytometry analyses of SIRPα expression from $AF647^+CD11b^+$ monocytes. **e**, Flow cytometry analyses of the binding efficiency of CD47-neutralizing antibodies to exosomes. $n = 3$ distinct batches of exosomes. **f**, Quantification of the number of exosomes per millilitre in the plasma of wild-type C57BL/6 mice ($n = 5$) versus CD47-knockout mice ($n = 7$). Data are mean ± s.e.m. $^*P < 0.05$, $^{***}P < 0.001$, one-way ANOVA (**b**, **e**) and unpaired two-tailed *t*-test (**f**). See accompanying Source Data.

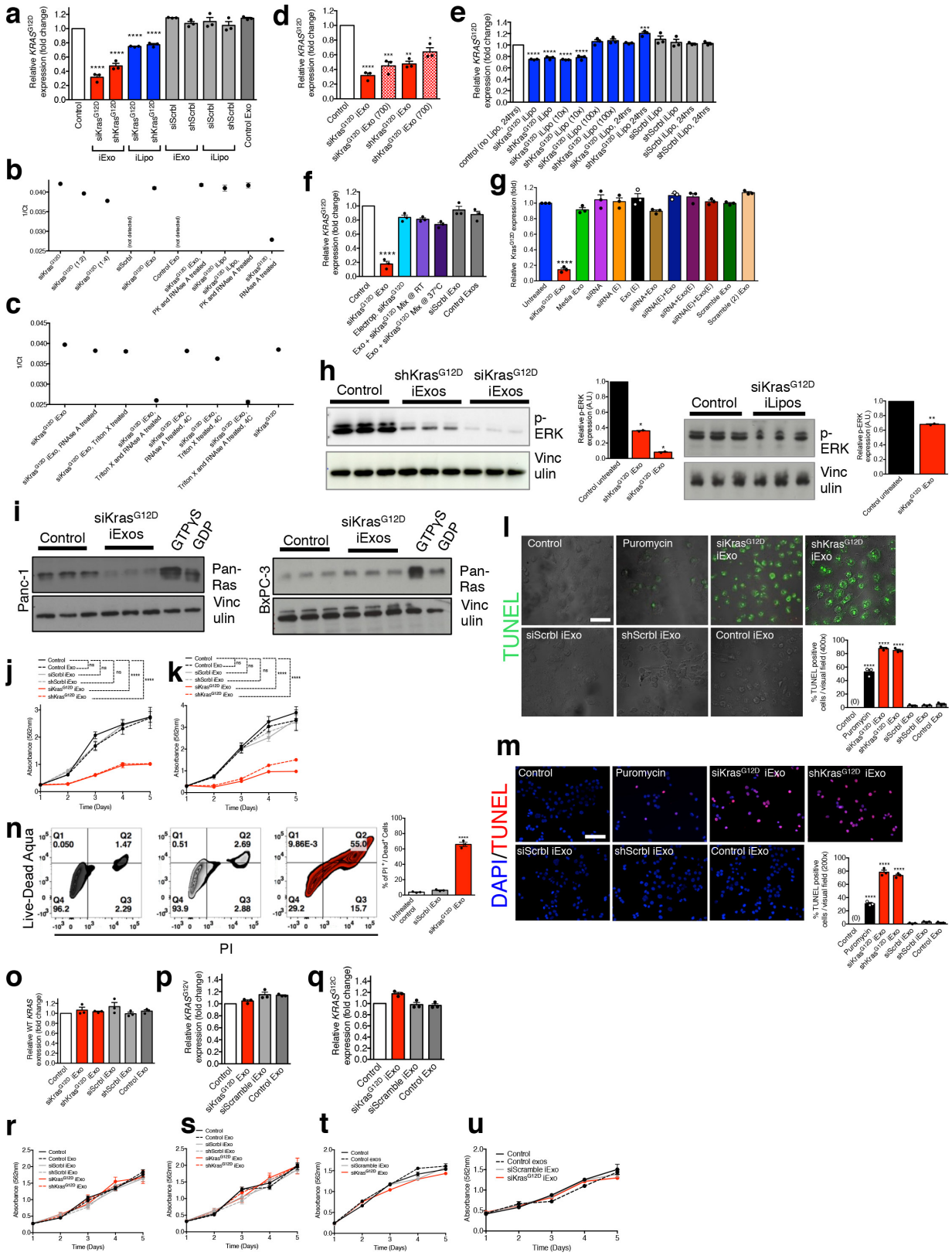

Extended Data Figure 4 | See next page for caption.

Extended Data Figure 4 | iExosomes specifically target KRAS^{G12D} expression. a, *KRAS^{G12D}* transcript levels in PANC-1 cells. $n = 3$ independent experiments. **b**, **c**, $1/C_t$ values from qPCR analysis under the listed conditions, to determine the loading efficiency of siRNA. Standards (siKras^{G12D}, 1:2 and 1:4 dilution): $n = 1$; experimental groups: $n = 3$ independent experiments. **d**, *KRAS^{G12D}* transcript levels in PANC-1 cells. $n = 3$ independent experiments. The experiments with 400 exosomes per cell are the same data shown in **a**. **e**–**g**, *KRAS^{G12D}* transcript levels in PANC-1 cells under the listed conditions. In all groups, $n = 3$ independent experiments. **h**, Western blotting in PANC-1 cells for p-ERK and vinculin. $n = 2$ independent experiments. **i**, RAS pull-down assay. **j**, **k**, PANC-1 cells MTT assay ($n = 5$ partitions of indicated treatments with 3 or 6 wells for each partition of treatment) (**j**) and a separate independent experiment (**k**). **l**, **m**, TUNEL assay ($n = 3$ distinct wells of PANC-1 cells) (**l**) and a separate independent experiment (**m**). **n**, Flow cytometry analysis of apoptosis in PANC-1 cells. Three different treatments were used to treat $n = 3$ distinct wells of cells. **o**, Wild-type *KRAS* transcript levels in BxPC-3 cells. $n = 3$ independent experiments. **p**, *KRAS^{G12V}* transcript levels in Capan-1 cells. $n = 3$ independent experiments. **q**, *KRAS^{G12C}* transcript levels in MIA PaCa-2 cells. $n = 3$ independent experiments. **r**, **s**, MTT assay in BxPC-3 cells ($n = 5$ partitions of treatment given to 3 wells each) (**r**) and a separate independent experiment (**s**). **t**, MTT assay in Capan-1 cells ($n = 3$ partitions of treatment given to 10 wells each). **u**, MTT assay in MIA PaCa-2 cells ($n = 3$ partitions of treatment given to 10 wells each). Data are mean ± s.e.m. $*P < 0.05$, $**P < 0.01$, $***P < 0.001$, $****P < 0.0001$, one-way ANOVA (for all, except **h**, iLipos), and two-tailed *t*-test (**h**, iLipos). See accompanying Source Data. For uncropped blots in **h** and **i**, see Supplementary Fig. 1.

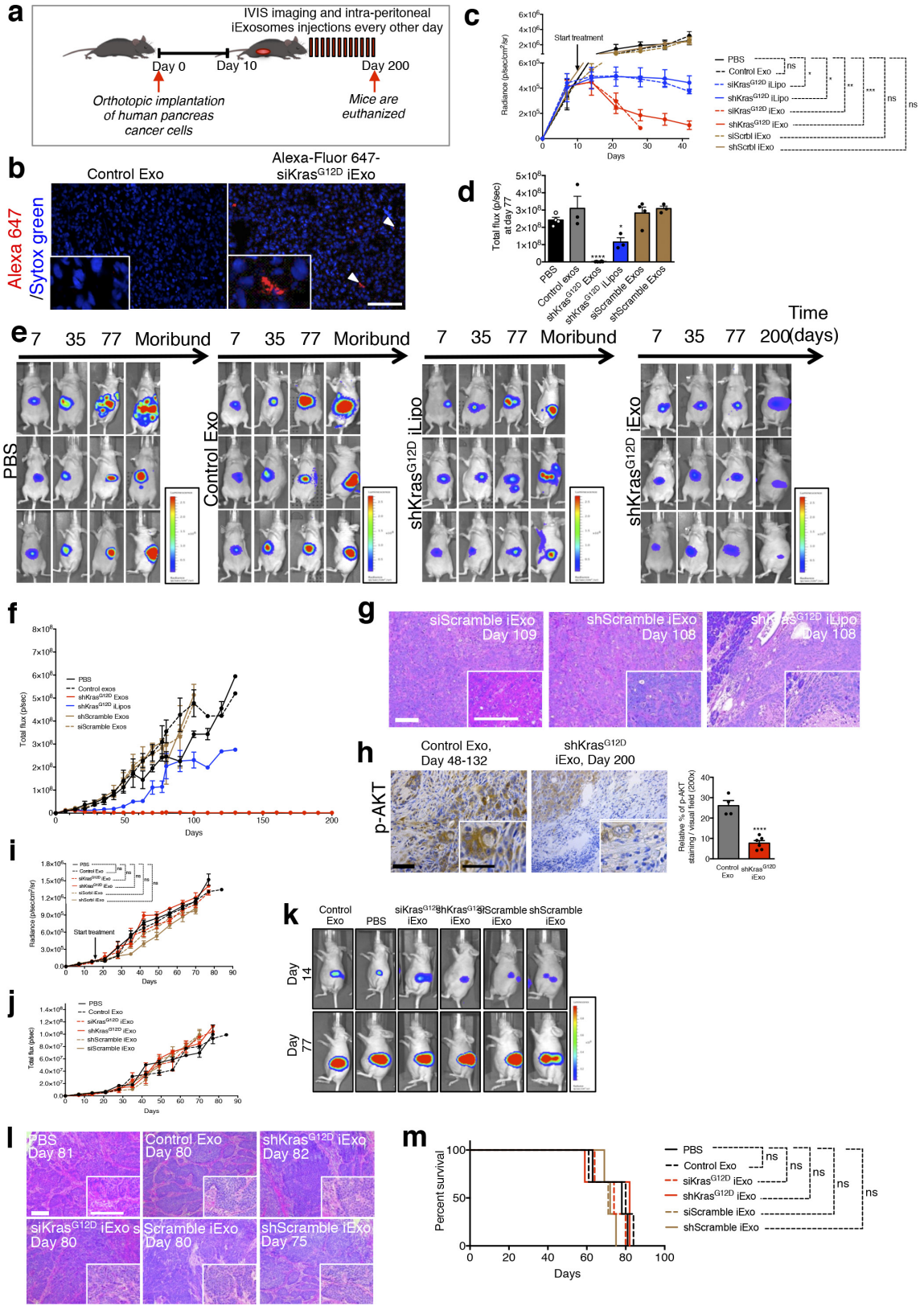

Extended Data Figure 5 | See next page for caption.

Extended Data Figure 5 | *Kras^{G12D}* RNAi-containing exosomes suppress PANC-1 but not BxPC-3 orthotopic tumour growth. a, Experimental scheme. **b**, Representative micrographs depicting accumulation of internalized AF647-tagged siRNA from exosomes. Scale bar, 100 μm. **c**, PANC-1 orthotopic tumour growth (an inset from data in Fig. 2c). $n = 6$ mice (PBS, control Exo); $n = 3$ mice (siKras^{G12D} iLipo, shKras^{G12D} iLipo); $n = 7$ mice (siKras^{G12D} iExo, shKras^{G12D} iExo); $n = 5$ mice (siScrbl iExo, shScramble iExo). Treatment groups were compared to PBS control at day 42 after cancer cell injection, or day 28 for siKras^{G12D} exosomes group. **d**, Tumour growth (bioluminescence) at day 77 (total flux). $n = 4$ mice (PBS, siScramble iExo); $n = 3$ mice (control Exo, shKras^{G12D} iLipo, shScramble iExo); $n = 6$ mice (shKras^{G12D} iExo). **e**, Luciferase activity at days 7, 35 and 77, and moribund stage or day 200 (shKras^{G12D} iExo) after cancer cell injection. Some of these panels are also shown in Fig. 2a. **f**, PANC-1 orthotopic tumour growth (bioluminescence) over time (total flux). $n = 7$ mice (PBS, shKras^{G12D} iExo); $n = 6$ mice (control Exo); $n = 4$ mice (shKras^{G12D} iLipo); $n = 5$ mice (shScramble iExo, siScramble iExo). **g**, Representative H&E staining of the PANC-1 orthotopic tumours. Scale bars, 100 μm. **h**, Representative micrographs (left) and quantification (right) of tumours immunostained for p-AKT. Scale bars, 100 μm. $n = 4$ mice (control Exo); $n = 6$ mice (shKras^{G12D} iExo). **i**, **j**, BxPC-3 orthotopic tumour growth (bioluminescence) over time. Radiance (**i**) or total flux (**j**). $n = 3$ mice per group. **k**, Luciferase activity at days 14 and 77 after cancer cell (BxPC-3) injection. **l**, Representative H&E staining of the BxPC-3 orthotopic tumours at the indicated experimental end points. Scale bars, 100 μm. **m**, Kaplan–Meier survival curve of BxPC-3 tumour-bearing mice. $n = 3$ mice per group. Data are mean ± s.e.m. $^{*}P < 0.05$, $^{**}P < 0.01$, $^{***}P < 0.001$, $^{****}P < 0.0001$, one-way ANOVA (**d**, **f**, **i**, **j**), unpaired two-tailed *t*-test (**c**, **h**) and log-rank Mantel–Cox test (**m**). See accompanying Source Data.

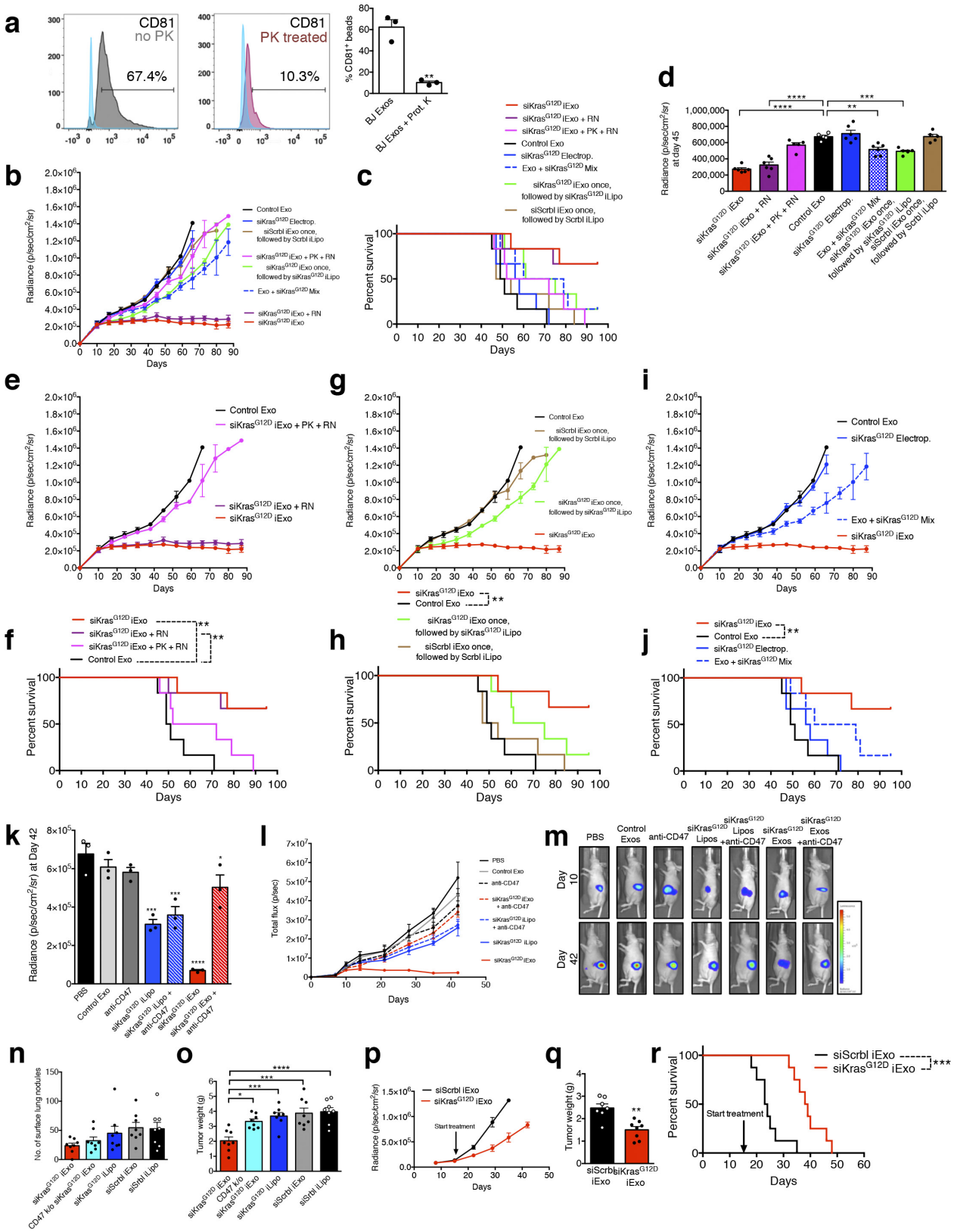

Extended Data Figure 6 | See next page for caption.

Extended Data Figure 6 | Anti-tumour response of iExosomes in orthotopic models. a, Flow cytometry analyses and quantification of CD81 in exosomes under listed conditions. $n = 3$ independent experiments. **b**, PANC-1 orthotopic tumour growth (bioluminescence) over time. $n = 6$ mice per group. **c**, Kaplan–Meier survival curve of PANC-1 tumour-bearing mice. $n = 6$ mice per group. **d**, Tumour growth (bioluminescence) at day 45. $n = 6$ mice per group. **e–j**, PANC-1 orthotopic tumour growth (bioluminescence) over time, depicting separate groups from **b** (**e**, **g**, **i**) and Kaplan–Meier survival curve, depicting the separate groups from **c** (**f**, **h**, **i**). $n = 6$ mice per group. **k**, Tumour growth (bioluminescence) at day 42. $n = 3$ mice per group. Experimental groups compared to PBS control. **l**, Growth of PANC-1 orthotopic tumours (bioluminescence) over time (total flux). $n = 3$ mice per group. **m**, Luciferase activity at days 10 and 42 after cancer cell (PANC-1) injection. **n**, Surface lung nodules of KPC689 mice. $n = 8$ mice per group. **o**, Tumour weights. $n = 8$ mice per group. siKras^{G12D} iExo group is compared to other treatment groups. **p**, Bioluminescent KPC689 orthotopic tumours in *nu/nu* mice. $n = 8$ mice per group. **q**, Tumour weights. $n = 8$ mice per group. **r**, Kaplan–Meier curve of KPC689 *nu/nu* mice. $n = 8$ in each group. Data are mean ± s.e.m. $^{**}P < 0.01$, $^{***}P < 0.001$, $^{****}P < 0.0001$, unpaired two-tailed *t*-test (**a**, **q**), ANOVA (**d**, **k**, **n**, **o**) and log-rank Mantel–Cox test (**c**, **e–j**, **r**). See accompanying Source Data.

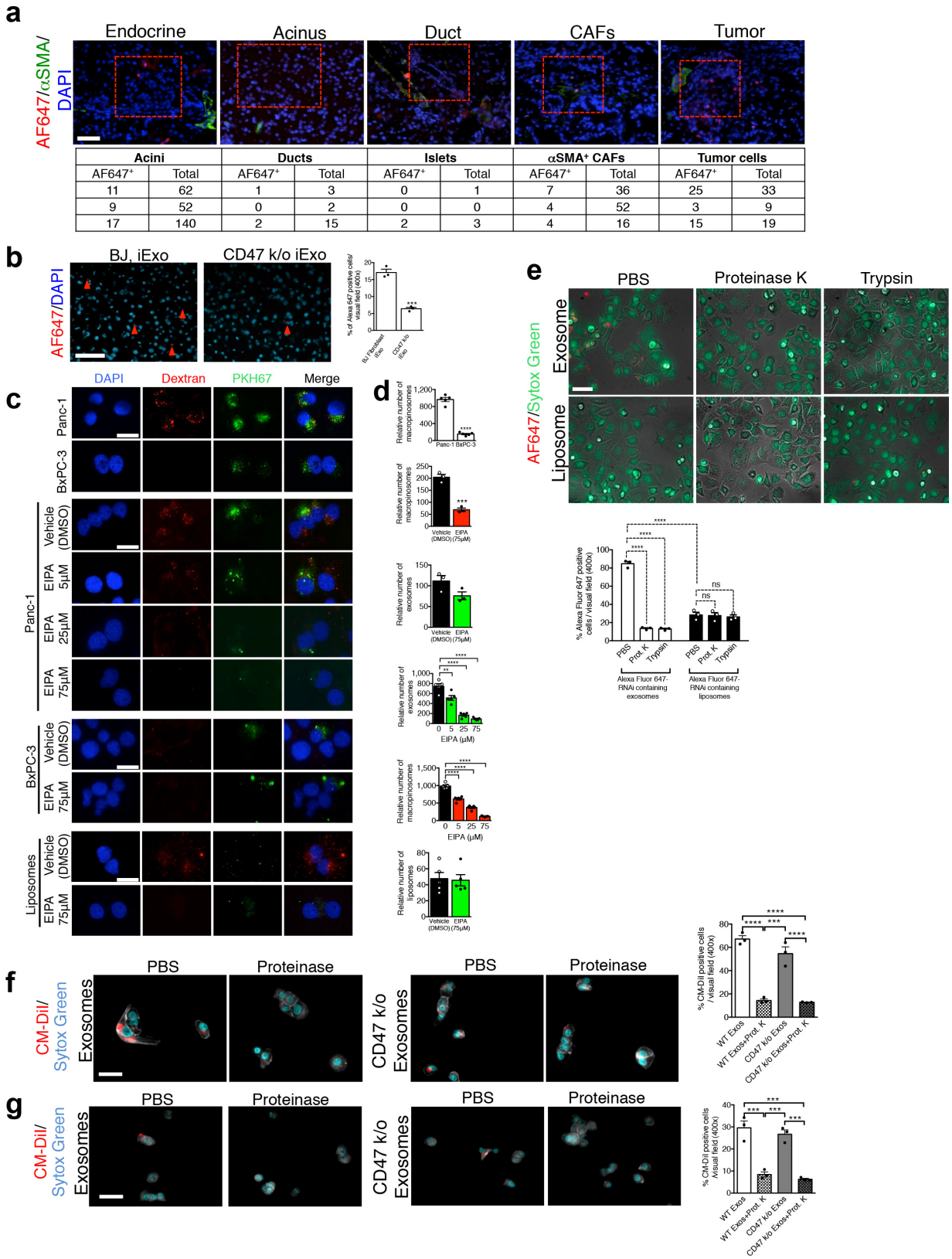

Acini		Ducts		Islets		αSMA⁺ CAFs		Tumor cells	
AF647⁺	Total	AF647⁺	Total	AF647⁺	Total	AF647⁺	Total	AF647⁺	Total
11	62	1	3	0	1	7	36	25	33
9	52	0	2	0	0	4	52	3	9
17	140	2	15	2	3	4	16	15	19

Extended Data Figure 7 | Pancreas localization and macropinocytosis promotes iExosome uptake into tumour cells. a, Representative images (top) and quantification (bottom) of pancreas structure in KTC mice injected with exosomes containing AF647-tagged siRNA. $n = 3$ mice. **b**, Representative images (left) and quantification (right) of pancreas of mice injected with the indicated conditions. $n = 3$ mice per group. **c**, Representative images for data in Fig. 3e–h. **d**, Quantification of macropinocytic and exosomes uptake (independent experiment, identical statistical analyses). **e**, Uptake of exosomes or liposomes containing AF647-tagged siRNA into PANC-1 cells. $n = 3$ independent experiments. **f**, Uptake of CM-DiI-tagged CD47-knockout versus wild-type exosomes in PANC-1 cells. $n = 3$ independent experiments. **g**, Uptake of CM-DiI-tagged CD47-knockout versus wild-type exosomes in BxPC-3 cells. $n = 3$ independent experiments. Scale bars, 100 μm (**a**, **b**, **e**, **f**) and 50 μm (**c**). Data are mean ± s.e.m. $^{*}P < 0.05$, $^{**}P < 0.01$, $^{***}P < 0.001$, $^{****}P < 0.0001$, one-way ANOVA (all except **b**) and unpaired two-tailed *t*-test (**b**). See accompanying Source Data.

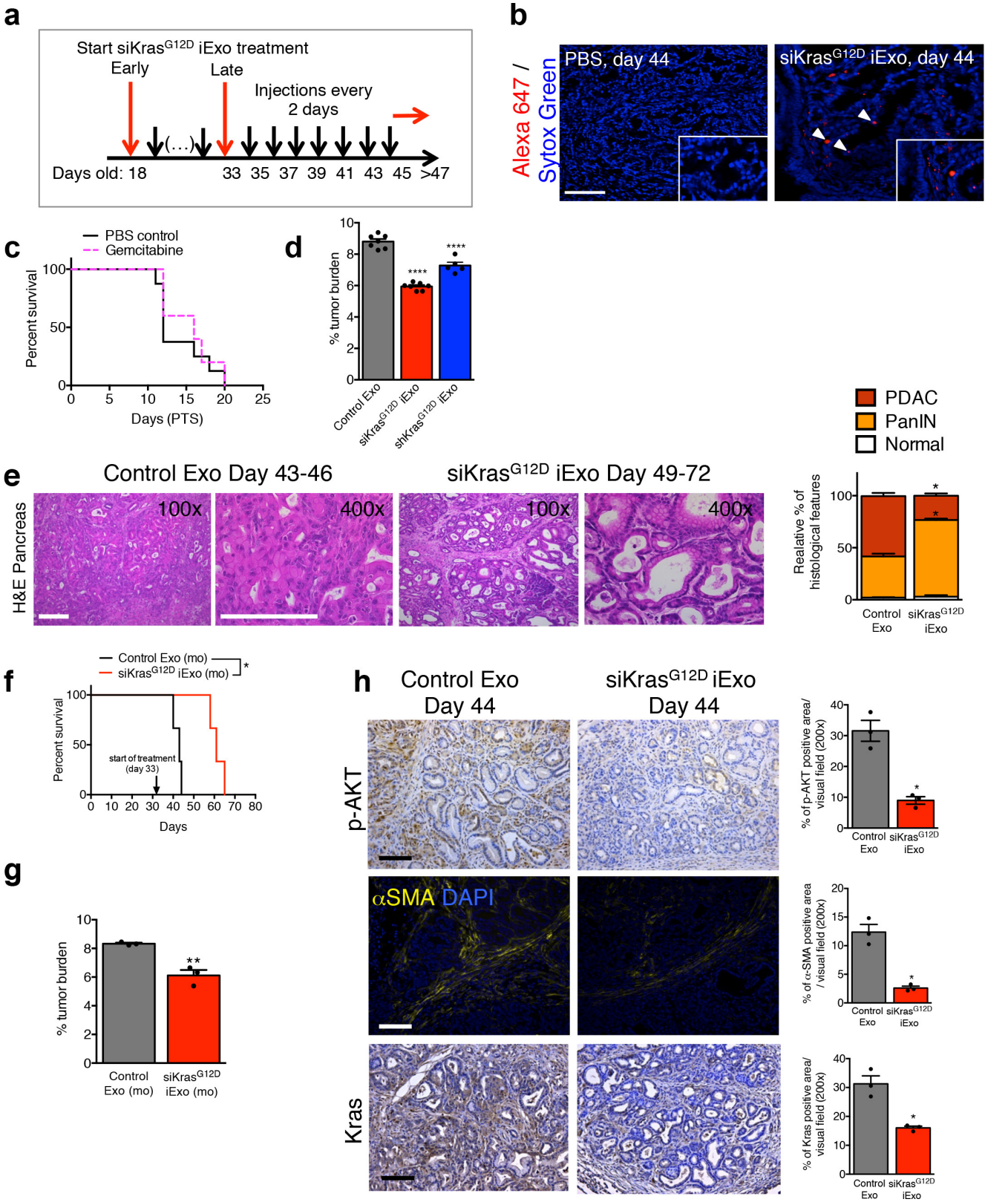

Extended Data Figure 8 | Treatment of KTC genetically engineered mice with iExosomes. a, Experimental scheme. **b**, Accumulation of internalized AF647-tagged siRNA from exosomes. **c**, Kaplan–Meier survival curve of KTC mice. $n = 8$ mice (PBS); $n = 5$ mice (gemcitabine). **d**, Tumour burden at the experimental end point. $n = 7$ mice (control Exo, siKras^{G12D} iExo); $n = 5$ mice (shKras^{G12D} iExo). **e**, H&E-stained tumours from KTC mice (left), and relative percentages in histological phenotypes (right). $n = 4$ mice per group. **f**, **g**, Kaplan–Meier curve of KTC mice (**f**) and percentage tumour burden (**g**). $n = 3$ mice per group. **h**, Representative micrographs of tumours immunostained for p-AKT, α-SMA and Kras from 44-day-old KTC mice in the indicated experimental groups. $n = 3$ mice per group. Scale bars, 100 μm (**b**, **e**, **h**). $^*P < 0.05$, $^{**}P < 0.01$, $^{****}P < 0.0001$, one-way ANOVA (**d**), unpaired two-tailed *t*-test (**e**, **g**, **h**) and log-rank Mantel–Cox test (**f**). See accompanying Source Data.

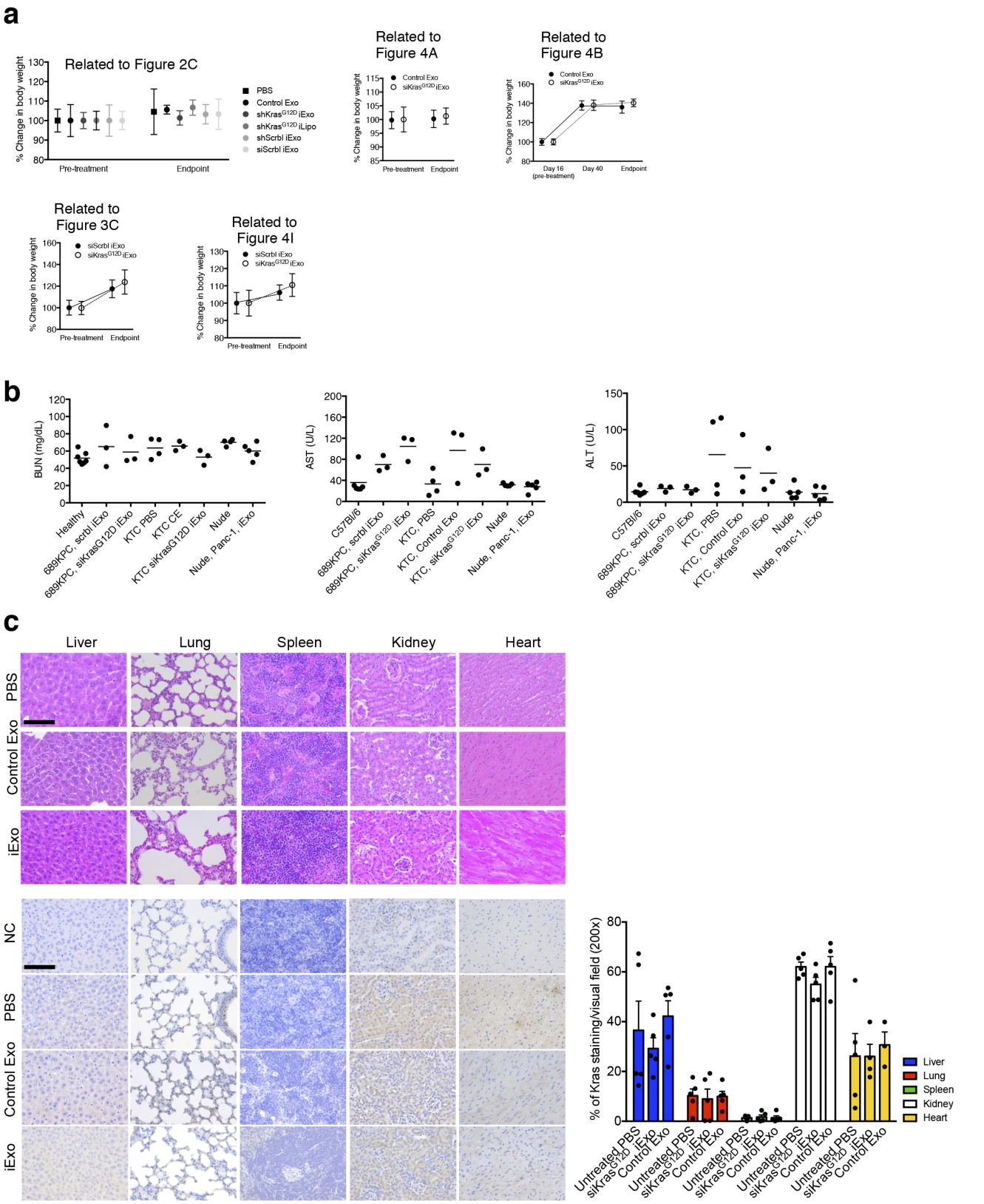

Extended Data Figure 9 | Evaluation of the cytotoxicity and off-target effect of iExosomes. a, Change in the percentage of mouse body weights, before and after treatment, in the listed groups and cohorts. One-way ANOVA (related to Figs 2c, 4a) and unpaired two-tailed *t*-test comparing the indicated groups at pre-treatment, day 40, and the experimental end point (related to Figs 3c, 4b, i). In all cases, there were no statistical differences observed. **b**, Mouse toxicity tests, consisting of blood urea nitrogen (BUN, aspartate transaminase (AST) and alanine transaminase (ALT) in the listed groups. One-way ANOVA comparing KTC mice, unpaired two-tailed *t*-test comparing nude mice, and unpaired two-tailed *t*-test comparing 689KPC mice. In all cases, there were no statistical differences observed. **c**, H&E and Kras immunostaining of the listed organs in KTC (early treatment) mice. $n = 3–5$ mice evaluated per organ. One-way ANOVA comparing the indicated groups in each organ. In all cases, there were no statistical differences observed. Data are mean ± s.e.m. See accompanying Source Data.

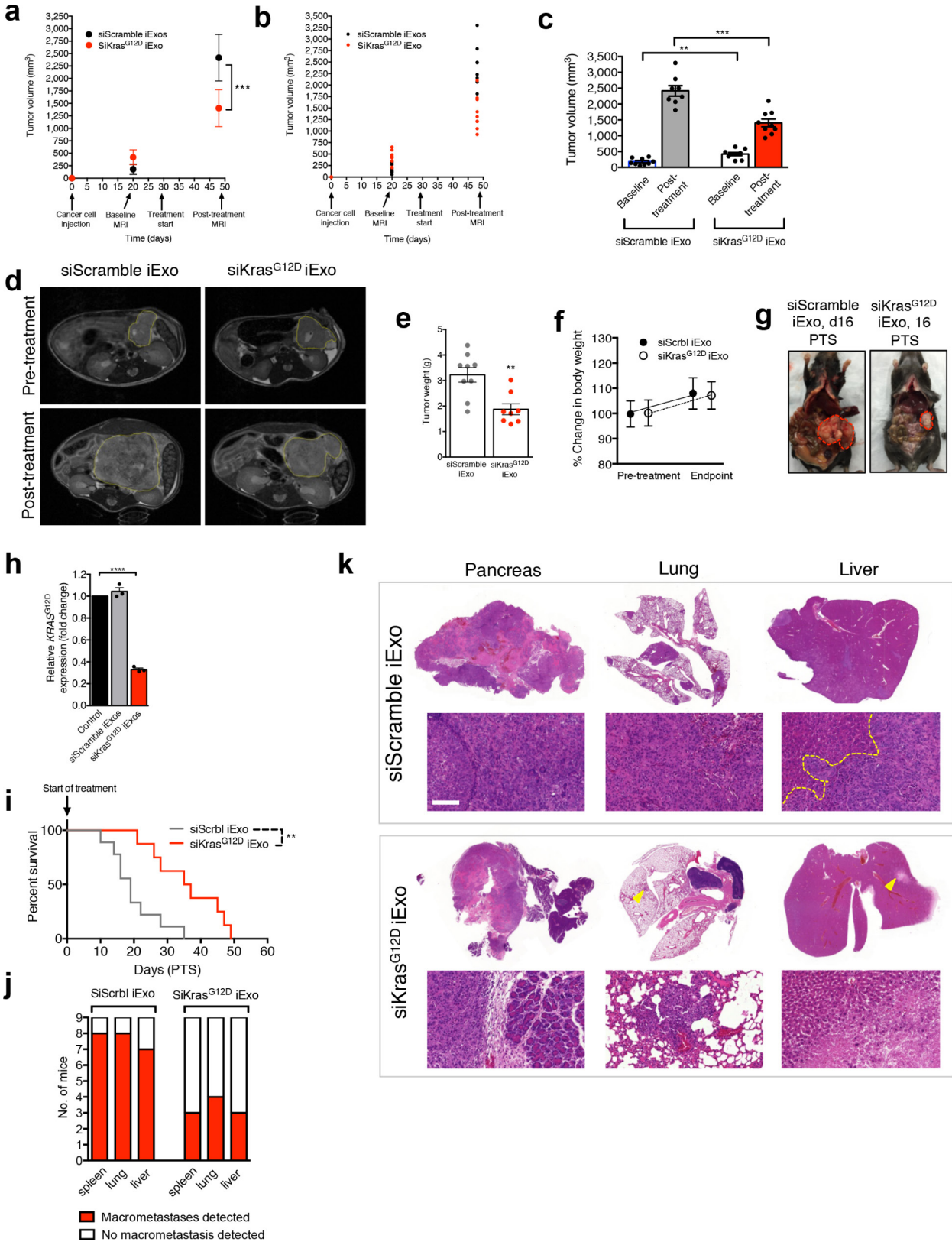

Extended Data Figure 10 | iExosomes suppress pancreatic cancer progression in the KPC orthotopic mouse model. a, **b**, MRI of KPC orthotopic tumours ($n = 9$ mice per group) (**a**) and each individual tumour (**b**). **c**, Tumour volume as measured by MRI. $n = 9$ mice per group. **d**, Representative axial images. **e**, Tumour weight at the experimental end point. $n = 9$ mice (siScrbl iExo); $n = 8$ mice (siKras^{G12D} iExo). **f**, Change in the percentage of mouse body weights, before and after treatment (end point). $n = 9$ mice per group. **g**, Representative gross images of two KPC orthotopic mice that died on day 16 post-treatment start (PTS) (siScrbl iExo) or was euthanized on day 16 PTS (siKras^{G12D} iExo). **h**, *Kras^{G12D}* transcript levels in KPC689 cells. $n = 3$ independent experiments. **i**, Kaplan–Meier survival curve of KPC orthotopic tumour-bearing mice. $n = 9$ mice (siScrbl iExo); $n = 8$ mice (siKras^{G12D} iExo). **j**, Macroscopic metastatic nodules. $n = 9$ mice per group. **k**, H&E-stained tissues. Data are mean ± s.e.m. $^*P < 0.05$, $^{**}P < 0.01$, $^{***}P < 0.001$, $^{****}P < 0.0001$, unpaired two-tailed *t*-test (**a**, **e**, **h**), one-way ANOVA (**c**), and log-rank Mantel–Cox test (**i**). See accompanying Source Data.